LASER INTERFEROMETER GRAVITATIONAL WAVE OBSERVATORY
-LIGO-
CALIFORNIA INSTITUTE OF TECHNOLOGY
MASSACHUSETTS INSTITUTE OF TECHNOLOGY

| | |
|---|---|
| **Technical Note**  **LIGO-T030234- 00-   D**    10/4/03 | |

# Modelling and Commissioning the Wavefront Sensing Auto-Alignment System of a Triangular Mode Cleaner Cavity

Matt Eichenfield

This is an internal working note
of the LIGO Project.

# Contents

# 1  Abstract

Interferometric gravitational wave detectors require stabilization of angular degrees of freedom to better than $10^{-8}$ radians rms, in addition to stringent length control tolerances. A powerful auto-alignment system has been developed to achieve this stability, and at its core is a sensing scheme called wavefront sensing. Using wavefront sensing to control the angular degrees of freedom of a triangular input mode cleaner cavity, the intensity of the light entering the main interferometer can be stabilized, noise sources are suppressed, and the long-term lock stability is increased. A time-domain model of the 40 Meter's 13.5 meter input mode cleaner wavefront sensing system will be presented. The choice of sensor configuration, actuators (PZT steering mirrors or cavity optics controllers), and servo filters, can be optimized using this model. While simultaneously checking the validity of the model against the real system, which has recently become operational, the model can be used to understand the more complicated behavior of the system and give direction as it is commissioned and optimized.

# 2  Keywords

LIGO, gravitational waves, laser interferometry, wavefront sensing, dynamical alignment of mirrors, alignment sensing and control, ASC, modal model, modal decomposition, triangular mode cleaner.

# 3 Introduction

Wavefront sensing is a scheme which can dynamically detect both the input coupling to and the orientation of a complex optical resonator cavity. It is the cornerstone of a complicated auto-alignment system which is used to enhance the stability of the cavity and give better noise performance.

The original plan for the mode cleaner auto-alignment system was to use steering mirror actuation, i.e. the input beam would be steered into the mode cleaner using piezoelectric transducer (PZT) controlled mirrors which control angle and position. The steering mirrors are then adjusted to minimize the wavefront sensing error signal. However, at the LIGO Livingston Observatory, experience suggests that this actuation scheme may not be ideal. As an alternative, they have suggested actuating on the suspended mode cleaner mirrors.

To address this and other problems, a Simulink model of the mode cleaner auto-alignment system has been created. The goal of the model is to answer questions about the difficulties of dynamic control including: is it necessary to use PZT controlled mirrors to steer the input beam into the mode cleaner; if the PZT mirrors are necessary, at what frequencies should feedback be devoted to the PZT mirrors and the suspended mode cleaner mirrors; are two quadrant photodiodes looking at the reflected field sufficient to control six angular degrees of freedom of three mirrors; if the input light is contaminated with excessive higher order modes which do not resonate in the mode cleaner, is it still possible to sense misalignment of the mirrors.

The basics of the detection/actuation scheme are simple:

1) Send phase modulated light into an optical resonator and look at the demodulated field reflected from the cavity with a photodiode (PD) capable of distinguishing displacement, such as a PD segmented into four quadrants.

2) Use lenses to "image" different parts of the mode cleaner (this is equivalent to tuning the Guoy phase).

3) Look for the production of higher order modes by their characteristic beat patterns as they interfere with the promptly reflected sidebands.

Thus the presence of higher order modes becomes an error signal for the auto-alignment system. Actuation is then used to eliminate the presence of the higher order modes.

It has been my personal experience that to fully understand wavefront sensing and auto-alignment systems, and thus the work explained in this paper, one must have a solid understanding of a myriad of concepts. In writing this paper, one of my goals has been to present the bulk of these concepts in a single document. In the hopes that future students will find it useful, I have included a lengthy introductory section that gives a full theoretical treatment of the concepts involved. Whenever possible, I have tried to add insightful explanations that allow an "intuitive" understanding of the workings of Alignment Sensing and Control (ASC). In addition, I have provided many detailed references to much more involved treatments of the topics.

# 4  Theoretical Background

## 4.1  Fundamental Modes of the Radiation Field Inside an Optical Cavity

Light that propagates inside a resonator spreads due to diffraction off the mirrors. However, it must not spread appreciably, or it will suffer large losses. Cavity radiation then, unlike plane and spherical waves, is characterized by its finite transverse extent. Despite this major difference, the properties of light in a cavity are best described in terms of its similarities to plane and spherical waves.

### 4.1.1  Gauss-Hermite Solutions: TEM$_{mn}$ Modes

When Maxwell's equations are decoupled, the magnitude of the electric field, **E**, can be written as the solution to the scalar wave equation. In free space, this becomes [1]

$$\nabla^2 E = \frac{1}{c^2}\frac{\partial^2 E}{\partial t^2} \, . \tag{1}$$

If a harmonic time dependence is assumed, i.e.

$$E(x,y,z,t) = E\left(x,y,z\right)e^{\pm i\omega t} \, , \tag{2}$$

then $E(x,y,z)$ satisfies the Helmholtz differential equation,

$$\nabla^2 E\left(x,y,z\right) + k^2 E\left(x,y,z\right) = 0 \, , \tag{3}$$

where $k = \omega/c$.

Furthermore, $z$ is chosen as the propagation direction by making

$$E(x,y,z) \rightarrow E(x,y,z)e^{-ikz} \tag{4}$$

If in addition, we enforce that partial derivatives with respect to $z$ higher than first order are neglected[2], i.e. all rapid variation with respect to $z$ is contained in the exponential in (4), then (3) becomes

$$\left(\frac{\partial^2}{\partial x^2} + \frac{\partial^2}{\partial y^2} - 2ik\frac{\partial}{\partial z}\right) E\left(x,y,z\right) = 0 \, . \tag{5}$$

This equation is separable, and the general solution to the wave equation (1) becomes

$$E\left(x,y,z,t\right) = \sum_{m,n=0}^{\infty} a_{mn} TEM_{mn} = \sum_{m,n=0}^{\infty} a_{mn} u_m\left(x,z\right) u_n\left(y,z\right) e^{-i(kz\pm\omega t)} \, . \tag{6}$$

Here the functions $u_m$ are the normalized Gauss-Hermite functions given by

$$
\begin{aligned}
u_m\left(x,z\right) \;=\; & \left(\frac{2}{\pi}\right)^{\frac{1}{4}} \left(\frac{1}{2^m\,m!\,w(z)}\right)^{\frac{1}{2}} H_m\left(\frac{\sqrt{2}x}{w(z)}\right) \\
& \exp\left(-x^2\Big(\frac{1}{w(z)^2} + i\frac{k}{2R(z)}\Big)\right) \exp\left(i\Big(m+\frac{1}{2}\Big)\eta(z)\right) ,
\end{aligned}
\tag{7}
$$

---

[1]The derivation of Maxwell's equations and their simplification to the scalar wave equation can be found in [1].

[2]Specifically: $kE' \gg E'' \ll k^2 E$. This is the equivalent of the paraxial approximation.

where $H_k$ is a Hermite polynomial and satisfies the ordinary differential equation

$$\frac{d^2 H_k}{ds^2} - 2s\frac{dH_k}{ds} + kH_k = 0 \,. \tag{8}$$

The first few Hermite polynomials are:

$$H_0(x) = 1, \quad H_1(x) = 2x, \quad H_2(x) = 4x^2 - 2 \,. \tag{9}$$

The auxiliary functions in (7) are defined as follows:

$$z_0 = \frac{\pi w_0^2}{\lambda} \,, \tag{10}$$

$$w(z) = w_0^2 \sqrt{1 + \left(\frac{z}{z_0}\right)^2} \,, \tag{11}$$

$$R(z) = z\left(1 + \left(\frac{z_0}{z}\right)^2\right) \,, \tag{12}$$

$$\eta(z) = \arctan\left(\frac{z}{z_0}\right) \,. \tag{13}$$

In these equations $\lambda = 2\pi/k = 2\pi c/\nu$ is the wavelength of light, and $w_0$ is the minimum spot size (the significance of these equations will be clarified in section 4.1.2).

The functions $u_m$ are normalized such that

$$\int\limits_{y=-\infty}^{y=+\infty} \int\limits_{x=-\infty}^{x=+\infty} u_m(x,z)u_n(y,z)\overline{u_m(x,z)u_n(y,z)}\,\mathrm{d}x\,\mathrm{d}y = 1 \,, \tag{14}$$

where the overbar denotes complex conjugation. This normalization condition, together with the fact that the Gauss-Hermite functions are orthogonal[3], ensures that in any plane perpendicular to the $z$-axis, the total amount of energy contained in each mode, TEM$_{mn}$, is equal to the absolute square of its coefficient, $a_{mn}$[4].

### 4.1.2 Physical Characteristics of the TEM$_{00}$ Mode

The $TEM_{00}$ mode, more commonly called a Gaussian beam, illustrates the vast majority of the properties of all Gauss-Hermite modes. Setting $m = n = 0$,

$$E_{00}(x,y,z) = \sqrt{\frac{2}{\pi}}\frac{1}{w(z)} \exp\left(-\left(x^2 + y^2\right)\left(\frac{1}{w(z)^2} + i\frac{k}{2R(z)}\right)\right)\exp\left(i\left(\eta(z) - kz\right)\right), \tag{15}$$

where only the harmonic time dependence has been excluded. The solution for the Gaussian beam can also be found by requiring that the solution to (3) be azimuthally symmetric [5].

---

[3]For a comprehensive discussion of the mathematical properties of Hermite polynomials with respect to the Gaussian weighting function, see [2].

[4]The definition of $a_{mn}$ is implicit in (6).

[5]See the derivation in [3], chapter 3.

Briefly, the Gaussian beam describes an azimuthally symmetric beam propagating in the positive z direction. Over 80% of the beam's energy is contained close to the axis of propagation in a hyperboloid of revolution, and in a given plane perpendicular to the axis, the transverse (radial) intensity distribution of the beam is a Gaussian whose width is equal to the width of the hyperboloid in that plane. The wavefronts of the beam are spherical, and in the far field the wavefronts look like those of a spherical point source at the origin. The phase of the beam is almost that of a plane wave, but there is a $z$-dependent phase, called the Guoy phase, that causes the beam to lead an equivalent plane wave to the right of the origin and lag it to the left.

The beam properties will be more thoroughly and easily explained after discussing the auxiliary functions defined in (10) through (13).

One can obtain the physical significance of $w(z)$ by examining the power in the Gaussian beam. The power is proportional to $|E_{00}|^2$; so

$$P_{00} \propto |E_{00}|^2 = \frac{2}{\pi} \frac{1}{w(z)^2} \exp\left( \frac{-2(x^2 + y^2)}{w(z)^2} \right) . \tag{16}$$

When $x^2 + y^2 = w(z)^2$, the value of the exponential is $1/e^2$. Thus, for every value of $z$, $w(z)$ is the radius of a circle in the x-y plane at which the power has fallen by a factor of $1/e^2$ compared with its value on the beam axis. This is why $w(z)$ is commonly referred to as the beam spot size or beam radius. The spot size, $w(z)$, makes a hyperboloid of revolution, like the one shown in Figure 1. The radius of the hyperboloid at any given z is given by (11).
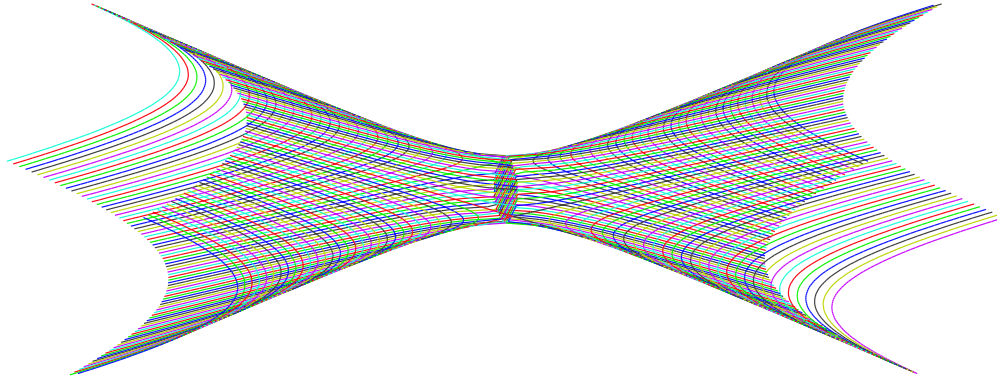


Figure 1: The point at which the power is $1/e^2$ its value on the axis forms a hyperboloid of revolution, which defines the beam's profile.

The minimum spot size, $w_0$, always occurs at $z = 0$, which is called the beam waist. Besides the wavelength of the radiation, the amplitude, and the choice of origin, the minimum spot size is the only free parameter needed to determine the field. It has two main consequences: first, since the beam size is always proportional to $w_0{}^6$, it scales the overall size of the beam; second, from (11) one gets that the asymptotes of the hyperboloid are given by $\pm w_0/z_0$, which becomes $\pm \lambda/\pi w_0$, using (10). Thus, the size of the waist determines the divergence of the beam: as $w_0$ is made small, the beam converges down to a smaller spot, but it also *converges and diverges* more quickly as you decrease $w_0$. These concepts are illustrated in Figure 2.

___
[6]See (11).
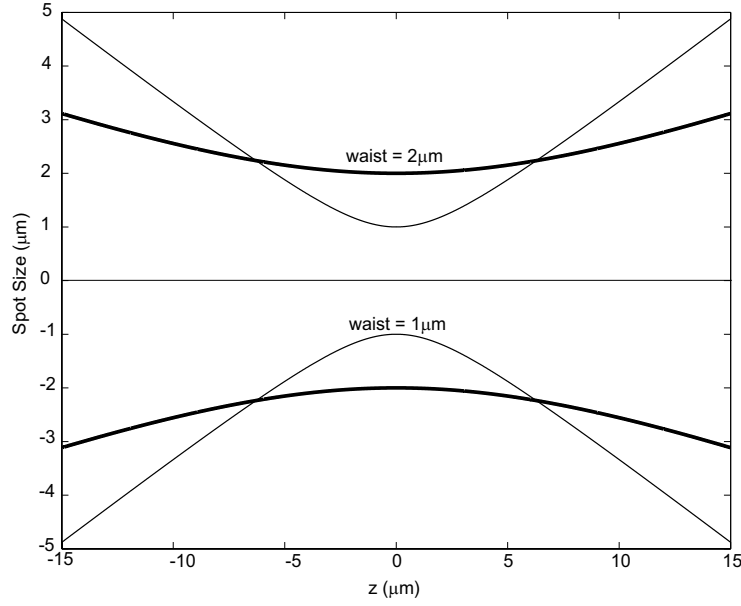
Figure 2: The divergence of two different beams of the same wavelength ($\lambda = 1\mu m$). Clearly, as the waist size is made smaller, the beam converges and diverges more rapidly. The exact numbers are not important, and are only meant to illustrate the divergence's dependence on spot size. In fact, a laser beam does not behave as usual when focused down to a spot size equal to the wavelength; in mathematical terms: this violates the paraxial approximation (see the footnote on page 5).

As mentioned above, in the far field the beam is asymptotic to the lines $\pm\lambda/\pi w_0$. The far field divergence angle, $\theta_D$, is defined to be the half-angle formed by these two lines, i.e.

$$\theta_D = \arctan(\lambda/\pi w_0). \tag{17}$$

This clearly illustrates that the divergence of the beam is inversely related to the waist size, $w_0$.

The Rayleigh length, $z_0$, is another important beam parameter, but this one is not independent of $w_0$, as can be seen from its definition in (10). The beam hyperboloid diffraction ideas also clearly illustrate the meaning of $z_0$: from (11), one can see that, in a distance $z_0$ on either side of the beam waist ($z = 0$), the spot size increases by a factor of $\sqrt{2}$ compared to the minimum size at the waist. Since the hyperboloid increases in size most slowly near the waist, $z_0$ can be thought of as the first distance over which there is a significant change in the beam spot; furthermore, in the far field, each increment in $z$ of $z_0$ increments the spot's radius by $w_0$.

In a given z-plane, the phase of the field is not constant; instead, the surfaces of constant phase are given by

$$\exp\left(-\left(x^2 + y^2\right)\left(i\frac{k}{2R(z)}\right)\right)\exp\left(i\left(\eta(z) - kz\right)\right) = \text{constant}. \tag{18}$$

The Guoy phase, $\eta(z)$, is defined in (13). It is a slowly varying component of the phase associated with propagation[7]. Naively, it may be viewed as the amount by which the beam would lag or lead an equivalent plane wave: at $z = 0$, where the Guoy phase is zero, a plane wave $e^{-ikz}$ would have equal propagation phase, and at $z = \pm\infty$ the Guoy phase is $\pm\pi/2$. In other words, the beam acquires a phase

---

[7]Guoy phase is not unique to Hermite-Gaussian beams; it is an effect common to all diffraction phenomenon.

shift of $\pi/2 - (-\pi/2) = \pi$ as it converges and diverges about the waist. The behavior of the Guoy phase is illustrated in Figure 3.
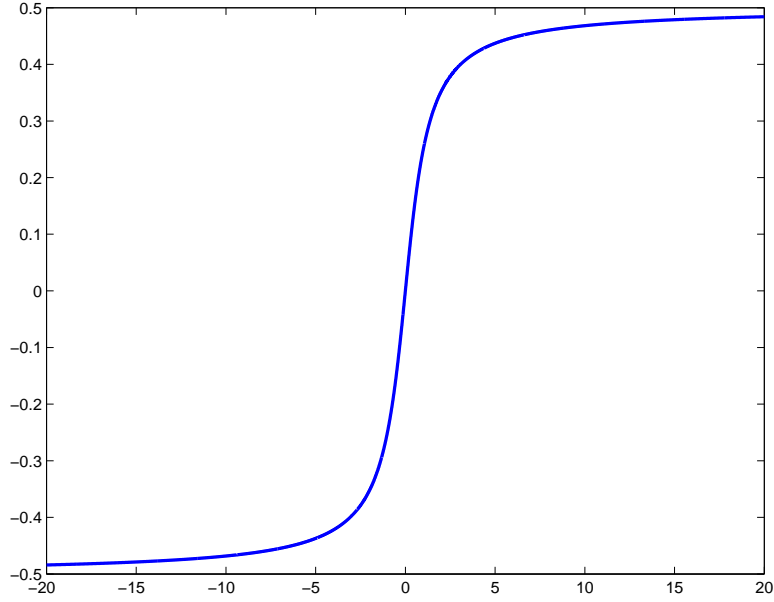


Figure 3: The Guoy phase, $\eta(z)$, is shown here. Notice the slow convergence to $\pm\pi/2$ as $z \to \pm\infty$. The x-axis is in units of the Rayleigh range, $z_0$, and the y-axis is in units of $\pi$ radians.

The Guoy phase actually determines the evolution of an arbitrary field distribution as it propagates through free space. Since it is the only phase term not common to the Hermite-Gaussian modes, it causes the spatial interference of these modes to vary in space. This will be discussed more thoroughly in section 4.2.

If the Guoy phase is ignored, the terms remaining in a surface of constant phase is

$$\exp\left(-ik\left(z + \frac{x^2 + y^2}{2R(z)}\right)\right) = \text{constant}. \tag{19}$$

To understand the meaning of these surfaces of constant phase, consider a spherical point source emitting spherically symmetric wave fronts of the form $e^{-ik\sqrt{x^2+y^2+z^2}}$. Since the Gaussian beam has a limited transverse extent, in general $z \gg \sqrt{x^2 + y^2}$, and the square root can be expanded in a Taylor series. To first order, the above exponential becomes $e^{-ik\left(z + \frac{x^2+y^2}{2z}\right)}$. If we identify the radius of curvature of the point source's waves as $z$, then comparing with (19), we see that the Gaussian beam has spherical wave fronts with radii of curvature given by $R(z)$.

The radius of curvature (ROC) of the wavefronts is not just $z$ but a complicated function of $z$ given by (12). At the waist, the ROC is $\pm\infty$ (depending on the direction of approach), which corresponds to a flat, planar wavefront. From the waist, the radius of curvature decreases in both directions until it reaches the planes $z = \pm z_0$, where the ROC reaches its minimum, $\text{ROC}_{\text{min}} = \pm 2z_0$. The ROC then asymptotically approaches the line $\text{ROC} = z$, i.e. in the limit that $|z| \gg z_0$, the ROC is equal to $z$, which means that the wavefronts appear to come from a spherical point source at the origin. This behavior is illustrated in Figure 4.
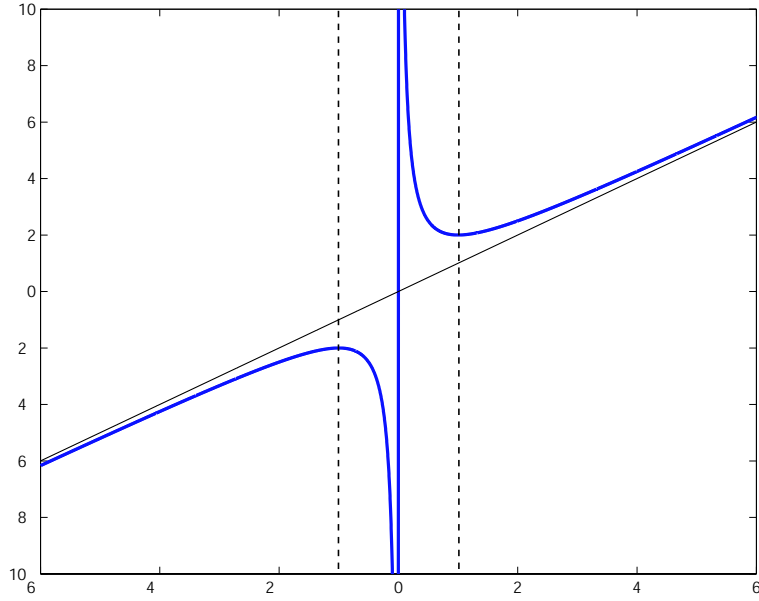
9

Figure 4: The function $R(z)$ is shown here. The dotted lines are the planes $z = \pm z_0$, where the absolute value of the ROC reaches its minimum, $2z_0$. The line $ROC(z) = z$ is shown to illustrate the asymptotic approach of $R(z)$. Both axes are in units of the Rayleigh range, $z_0$.

With the auxiliary equations, (10) through (13), defined in the above paragraphs, the behavior of the Gaussian beam can be summarized as follows:

1) the transverse profile of the beam is a Gaussian whose width is $w(z)$;

2) in order to conserve energy, the increasing width of the beam is balanced by the factor of $1/w(z)$;

3) the phase of the beam is much like a plane wave, but the Guoy phase, $\eta(z)$, slowly changes the phase as it travels;

4) the quadratic transverse dependence of the phase creates spherical wavefronts with the ROC given by $R(z)$.

These properties are illustrated in Figure 5.

### 4.1.3   The Action of Focusing Elements on a Gaussian Beam

An ideal lens does exactly one thing: when a spherical wavefront with ROC $= R_1$ is incident along the axis of the lens of focal length $f$, it is transformed by the lens into a different spherical wavefront with ROC $= R_2$ such that $1/R_1 + 1/R_2 = 1/f$, which is just the Gaussian lens equation [3].

In this context, it is not complicated to understand how a lens transforms a Gaussian beam. There are essentially two requirements that must be met: the radius of curvature of the input beam at the lens is transformed according to the Gaussian lens equation above, and the spot size on either side of the lens will be exactly the same. These two conditions determine what the properties of the Gaussian beam will be on the other side because there is only one solution whose radius of curvature and width can satisfy those criteria at a given position in space.
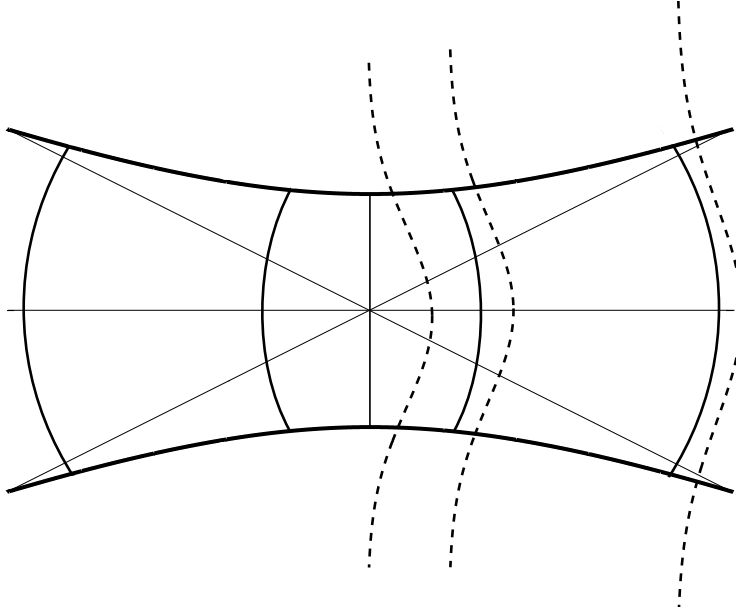
10

Figure 5: The behavior of the Gaussian beam is summarized here: the hyperbolic curves correspond to the beam profile and the local directions of propagation; the dark curved lines represent the spherical phase fronts of the beam given by $R(z)$ (note the flat wavefront at the waist); the dashed gaussian curves represent the transverse field distribution in a given $z$-plane; and the light straight lines indicate the asymptotic (far-field) beam propagation.

The equations that completely describe the transformation are easily derived in terms of the auxiliary parameter

$$Q(z) \equiv \frac{\pi}{\lambda} w(z)^2 = z_0 \left( 1 + \left( \frac{z}{z_0} \right)^2 \right) . \tag{20}$$

Note the symmetry of $Q(z)$ and $R(z)$ (see (12)). At the lens, the width, $w(z)$, does not change; so, neither does $w(z)^2$. Since $Q(z)$ and $w(z)^2$ are related by a constant, then $Q(z)$ does not change at the plane of the lens. This will simplify the calculations below.

We will now derive the equations that transform a Gaussian beam at a lens of focal length $f$ positioned at $z = z_1$, an arbitrary point along the beam path. Let the input beam have a waist at $z = 0$ and a Rayleigh range, $z_0$, equal to $z_{00}$. Let the outgoing beam have its waist at $z = z_w$ and a Rayleigh range equal to $z_{01}$. If the input beam and output beam have a ROC equal to $R$ and $R'$ respectively and values of $Q(z)$ equal to $Q$ and $Q'$ respectively, then using the constraints on R and Q, we have the following equations:

$$Q = Q', \tag{21}$$

$$R' = \left( \frac{1}{R} - \frac{1}{f} \right)^{-1} , \tag{22}$$

$$Q = z_{00} \left( 1 + \left( \frac{z_1}{z_{00}} \right)^2 \right) , \tag{23}$$

$$Q' = z_{01} \left( 1 + \left( \frac{z_w - z_1}{z_{01}} \right)^2 \right) , \tag{24}$$

11

$$R = z_1 \left( 1 + \left( \frac{z_{00}}{z_1} \right)^2 \right) , \tag{25}$$

$$R' = -(z_w - z_1) \left( 1 + \left( \frac{z_{01}}{(z_w - z_1)} \right)^2 \right) . \tag{26}$$

These equations can be solved (although not trivially) to yield the outgoing beam's Rayleigh range and the position of its waist:

$$z_{01} = \frac{z_{00}}{\left( 1 - \frac{z_1}{f} \right)^2 + \left( \frac{z_{00}}{f} \right)^2} \quad \text{and} \tag{27}$$

$$|z_w - z_1| = \frac{f}{1 + \left( \frac{f}{z_{00}} \right)^2 + \left( \frac{z_1}{z_{00}} \right)^2 \left( 1 - \frac{2f}{z_1} \right)} \left[ 1 + \left( \frac{z_1}{z_{00}} \right)^2 \left( 1 - \frac{f}{z_1} \right) \right] , \tag{28}$$

where the absolute value sign is used because the waist can be either real or virtual, corresponding to a waist after or before the lens respectively. Thus the output beam is entirely specified by shifting the coordinates of (15) by $z \to z - z_w$ and using the parameter $z_{01}$ as the Rayleigh range.

The Guoy phase has thus far not been mentioned, but it is quite a simple matter to discuss now that the above equations have been given. The phase of any electric field must be continuous; so, the Guoy phase must be matched on either side of the lens. From the waist to the lens, the input beam acquires a Guoy phase of $\eta = \arctan(z_1/z_{00})$. After the lens, both the position of the waist and the Rayleigh range have changed. Propagating from $z_1$ to some arbitrary position $z'$ will increment the Guoy phase by

$$\eta' = \arctan \left( \frac{z' - z_w}{z_{01}} \right) - \arctan \left( \frac{z_1 - z_w}{z_{01}} \right) , \tag{29}$$

where all the parameters have been defined above.

In the paraxial approximation, a mirror acts on a spherical wavefront in exactly the same way that a lens does, except that a mirror reverses the direction of propagation. Therefore, one can use all the ideas and equations above with the lens' focal length, $f$, replaced by half the mirror's radius of curvature.

For further discussion of these topics see chapter 3 in [3] or the section in [4] on Guoy phase telescopes.

### 4.1.4 Physical Characteristics of Higher Order Modes

When either $m \neq 0$ or $n \neq 0$, the radiation is no longer a simple Gaussian beam as described in section 4.1.2; instead, the field becomes one of the more complicated Gauss-Hermite modes given by

$$\text{TEM}_{mn} = u_m(x, z) u_n(y, z) e^{-ikz} , \tag{30}$$

where the function $u_m(x, z)$ is defined in (7).

There are two major differences between the Gaussian beam and its Hermite-Gaussian counterparts: the first is that the transverse dependence is no longer a simple Gaussian, and the second is that the Guoy phase accumulated per unit length is larger.

The transverse dependence of the electric field becomes the product of two Hermite polynomials and the familiar Gaussian. This has some profound consequences:

1) the transverse dependence is no longer symmetric with respect to x and y;

2) as the mode indices increase, the majority of the power in the beam becomes concentrated further and further from the axis, the result of which is that the $\text{TEM}_{00}$ mode is the narrowest of the Gauss-Hermite modes, and

3) for each $\text{TEM}_{mn}$ mode, there are $m+n$ nodal lines in the transverse plane along which the electric field (and thus the power) is identically zero.

Figure 6 shows the transverse extent of several Hermite-Gauss modes in a given plane.
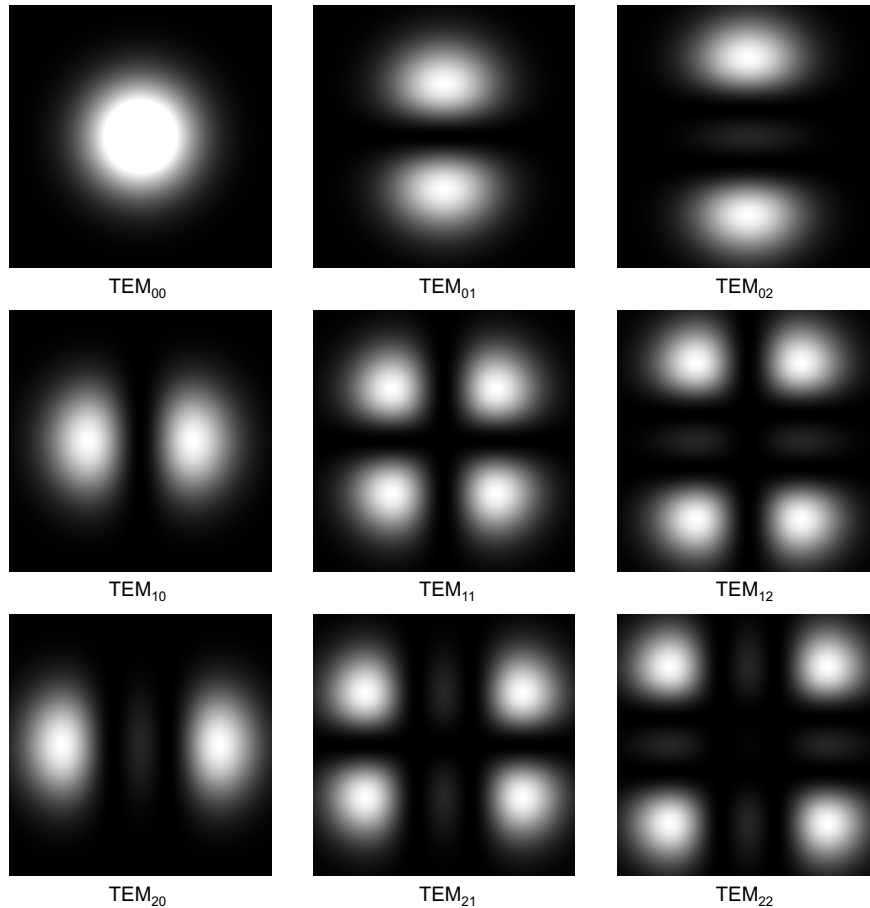
Figure 6: Transverse power distributions of several Hermite-Gauss modes in an arbitrary $z$-plane. Key points to note are the lack of x-y symmetry when $m \neq n$, the increase in off-axis power with increasing index, and the nodal lines. Actual photographs of these and other modes can be found in figure 3-4 of [3]

As the beam propagates, the Hermite polynomial spreads due to the factor of $1/\sqrt{w(z)}$ in the argument of the polynomial. This spreading is exactly right to guarantee that the transverse field/power dependence only scales up or down with changing $z$; the shape itself is constant.

From (13), one can see that the Guoy phase accumulated by the $\text{TEM}_{mn}$ mode is $(m+n+1)\eta$. This means that between any two points, the higher order mode is shifted in phase by a factor of $m+n$ more than the Gaussian beam. This extra Guoy phase shift has profound consequences, especially in the context of cavity resonance. This concept will be discussed in detail in section 4.1.5.

13

Besides the transverse field dependence and extra Guoy phase, the higher order modes are essentially identical to the Gaussian beam. In particular, all the auxiliary functions discussed in section 4.1.2 are almost exactly the same and have similar consequences: there is still a hyperboloid of revolution, although the circle defined by $w(z)$ now contains less than $1 - 1/e^2$ of the power; the wavefronts are still spherical with radii of curvature exactly the same as those of the Gaussian; and there is still a $z$-dependent Guoy phase.

### 4.1.5 TEM$_{mn}$ as Eigenmodes of an Optical Resonator

Consider the freely propagating (left to right) TEM$_{00}$ mode shown in Figure 5. If at some point along the path, the beam encounters a mirror whose ROC and center of curvature are equal to the those of the beam's spherical wavefront at that point, it will be perfectly retro-reflected. If a second mirror is also placed with matching ROC and center of curvature at a second point along the beam path, it will again be retro-reflected, making an exact spatial replica of itself as it bounces back and forth between the two mirrors. This scenario is illustrated in Figure 7.
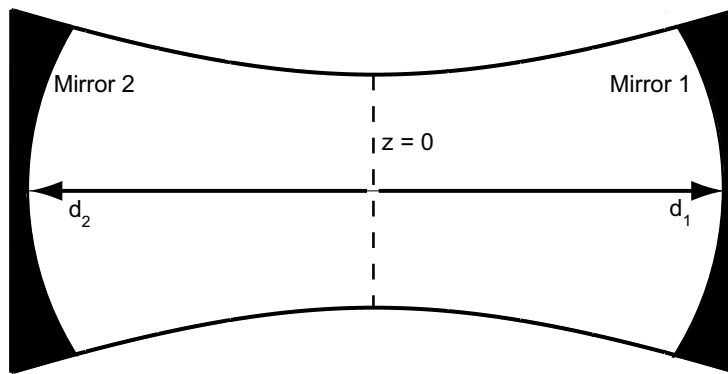


Figure 7: A resonator is created by placing two mirrors along the beam's path at points where their ROCs and centers of curvature match those of the propagating beam's wavefronts. In practice, the mirrors would be made much larger than the beam spot size to avoid large round trip losses.

As the beam bounces back and forth, it is superposed on top of itself many times. Thus, to avoid destructively interfering itself out of existence, the beam's phase must complete an integer number of full cycles, $2\pi$ radians, every round trip. The phase not only depends on the wavelength, as it would for a plane wave; the Guoy phase, $\eta(z)$, must also be taken into account. Remembering that the beam changes its direction of propagation on every bounce, the total round trip phase, $\phi_{rt}$, becomes

$$\phi_{rt} = 2(n+m+1)\left(\arctan\left(\frac{d_1}{z_0}\right) - \arctan\left(\frac{-d_2}{z_0}\right)\right) - 2k(d_1 - (-d_2)) , \qquad (31)$$

14

where $d_2$ is to the left of the waist, as shown in Figure 7. A given mode is said to be resonant, and thus an *eigenmode* of the cavity, if $\phi_{rt} = 2\pi q$, $q \in$ Integers; this statement is called the resonance condition.

One can, in fact, run the argument backwards. If one places two curved mirrors at arbitrary positions in space, only modes that propagate between the centers of curvature of the mirrors and satisfy the resonance condition will be able to propagate with minimal losses. The spatial properties of these modes can be easily calculated using resonator algebra.

Resonator algebra is nothing more than enforcing the fact that the ROC of an eigenmode must be equal to the ROC of any mirror which it encounters along its path, this condition is independent of mode indices. Consider the simple case where $d_2 = -d_1$, the radii of curvature of the two mirrors are equal, and both mirrors have their concave sides facing one another. In this case, the beam waist must lie halfway between the two mirrors (i.e. at $z = 0$). Let $d = |d_1| = |d_2|$, and let R be the radius of curvature of both mirrors. Using 12 we have the following equations:

$$R = d\left(1 + \left(\frac{z_0}{d}\right)^2\right) \tag{32}$$

$$-R = -d\left(1 + \left(\frac{z_0}{d}\right)^2\right). \tag{33}$$

These two equations are identical for a symmetrical resonator, and either one can be solved for $z_0$; one obtains

$$z_0^2 = (R - d)d. \tag{34}$$

Once $z_0$ has been obtained from the above equations[8], one can find which TEM$_{mn}$ modes satisfy the resonance condition by choosing a wavelength. These modes are the eigenmodes of the cavity.

All modes for which $m + n = $ constant will have the same resonance condition; thus, when one such mode is resonant with a particular wavelength, all are resonant. In general, for a given wavelength, no modes will be resonant. Moreover, when a given mode is resonant, modes with different indices will in general not be[9].

In most of the above discussion, the word resonance has been used in a manner that suggest only modes that exactly satisfy the resonance condition will propagate. This is not strictly true; in fact, the resonators discussed above are Fabry-Perot interferometers, and the propagation through a cavity is determined by the equations governing a Fabry-Perot. One thing can be said for sure though: modes which do not satisfy the resonance condition will suffer much larger losses than those that do. These ideas will be clarified in section 4.3.1.

## 4.2 Modal Decomposition

Modal decomposition is a powerful technique that allows one to analyze the misalignment of a resonant optical cavity[10]. One can do away with geometric considerations like tilted and offset beams; instead, one analyzes these cases in terms of the eigenmodes of the perfectly aligned cavity. Using the completeness and orthogonality of the Hermite-Gauss modes, one can decompose misalignment into the production of higher order cavity modes.

---

[8]For explicit details on how to perform these calculations when the above conditions are not met, see section 4.3 of [3].

[9]A full discussion of resonance conditions can be found in section 4.6 of [3].

[10]The pioneering paper on this subject is [5].

To see how this works, consider the case of a $TEM_{00}$ mode offset in the x direction; it will be shown in section 4.2.5 that this can be decomposed into the original $TEM_{00}$ mode with no offset plus a small amount of $TEM_{10}$ that is proportional to the amount of offset. Figure 8 shows this decomposition graphically.
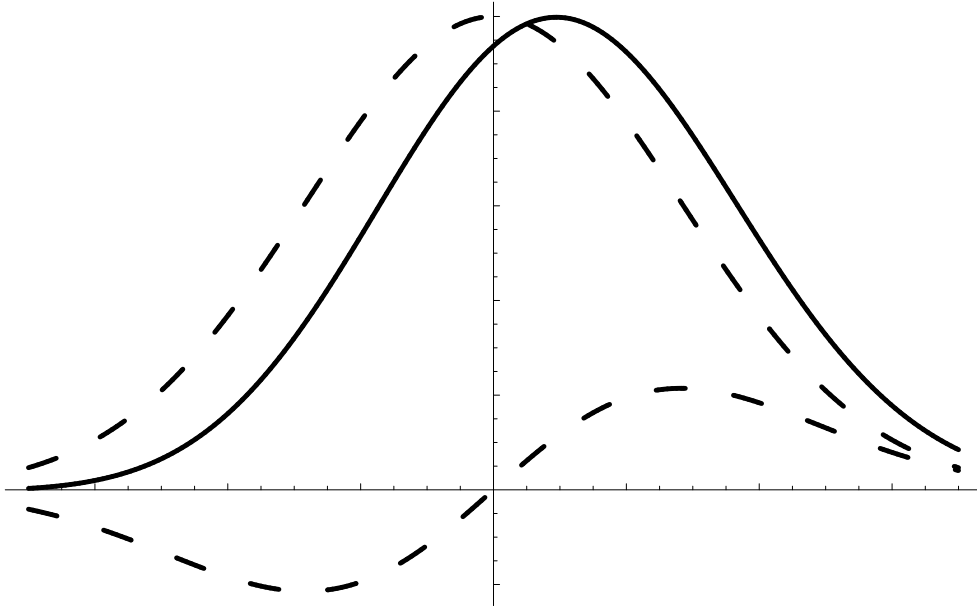


Figure 8: A shifted eigenmode is decomposed into unperturbed cavity eigenmodes. The two symmetric lines represent unperturbed $TEM_{00}$ and $TEM_{10}$ cavity eigenmodes. The third line is their sum, which is an offset $TEM_{00}$.

Once the decomposition has been performed, there are simple equations that describe the propagation of the eigenmodes. The process is easy to make recursive; so it is no more complicated for a beam misaligned multiple times in different locations than the trivial case illustrated above. The real power of this kind of analysis is that it can be treated by usual methods of linear algebra as will be shown in Section 4.2.3.

### 4.2.1 The Modal Model

One normally thinks of radiation in terms of an equation that describes the electric field's spatial and temporal properties at all points in space and at all points in time. The beauty and simplicity of the modal model is due to its departure from this description of radiation.

The modal model describes the electric field at any point in space and time as a set of complex amplitudes. These amplitudes describe the magnitude and *relative* phase of all $TEM_{mn}$ modes; in other words, only the set of $a_{mn}$ from (6) are necessary to describe the field. Thus, the modal model is not a spatial description of the field at all, but it is trivial to convert from one description to the other.

### 4.2.2 Propagation and Guoy Phase

Consider an arbitrary set of eigenmodes as they propagate through space. The only change in the amplitudes from one point to another is due to the Guoy phase[11]. If the beam waist is at $z = 0$, then between any two points in space (say from $z_1$ to $z_2$) the change in Guoy phase is

$$\eta(z_2, z_1) = \arctan\left(\frac{z_2}{z_0}\right) - \arctan\left(\frac{z_1}{z_0}\right) \tag{35}$$

for any given mode, TEM$_{mn}$. If one defines $a_{mn}$ and $a'_{mn}$ to be the amplitudes at $z = z_2$ and $z = z_1$ respectively, then

$$a'_{mn} = (m + n + 1)\, \eta(z_2, z_1) a_{mn} \,. \tag{36}$$

This is a very simple equation, but it contains all the information necessary to propagate a given set of amplitudes to any point in space[12]. This simplicity is really quite surprising. A demonstration of the wealth of information that the Guoy phase propagator contains can be found in [6], section 4.1.5, where it is shown that after reflecting off a tilted mirror, the Guoy phase is responsible for a laser beam's propagation in the direction given by the law of reflection; it combines two modes travelling straight ahead in such a way that their maximum power travels in the reflected ray direction.

### 4.2.3 Formalism

First and foremost, general definitions will be made *here*. Different notations abound in the literature; we will use the notation found in [6], which is the notation followed in the e2e simulation package used ubiquitously by the LIGO Scientific Community. The following equations define the propagating electromagnetic field:

$$E(x, y, z, t) = \exp\left(i\omega t\right) \cdot E(x, y, z), \tag{37}$$

$$E(x, y, z) = \sum a_{mn} \cdot Prop\left(z, \overline{z}\right) \cdot U_{mn}(x, y, z), \tag{38}$$

$$Prop\left(z, \overline{z}\right) = \exp\left[-ik \cdot (z - \overline{z})\right] \cdot \exp\left[i(m + n + 1) \cdot \left(\eta_{00}(z) - \eta_{00}(\overline{z})\right)\right], \tag{39}$$

$$U_{mn}(x, y, z) = u_m(x, z) \cdot u_n(y, z), \tag{40}$$

$$\eta_{00}(z) = \arctan\left(z/z_0\right), \quad \text{and} \tag{41}$$

$$u_m(x, z) = \left(\frac{2}{\pi}\right)^{\frac{1}{4}} \cdot \left(\frac{1}{2^m\, m!\, w(z)}\right)^{\frac{1}{2}} \cdot H_m\left(\frac{\sqrt{2}x}{w(z)}\right) \exp\left(-x^2\left(\frac{1}{w(z)^2} + i\frac{k}{2R(z)}\right)\right). \tag{42}$$

Here, $\overline{z}$ is the position of the waist. Note the *change in the definition of $u_m$* from (7); the contribution from the Guoy phase has been left off and included instead in the propagator. This is a subtle but important change. It is part of the paradigm shift made necessary by the modal model; one focuses on the set of amplitudes and how they transform from one point to another instead of a solution to the wave equation at every point in space.

The basic problem in modal decomposition will be illustrated by considering the case of an offset TEM$_{00}$[13] mode. Suppose we offset the mode by an amount $h$ in the $x$ direction. In other words,

---

[11]The factors $w(z)$ and $R(z)$ obviously change as well, but they change in exactly the same way for *all* modes. Thus, they do not need to be considered here.

[12]In fact, the bulk length phase $k(z_2 - z_1)$ has been ignored because it is the same for all modes. It will be stated explicitly when the bulk length phase must be taken into account

[13]TEM$_{mn}$ and $U_{mn}$ are essentially interchangeable.

$TEM_{00}(x, y, z) \rightarrow TEM_{00}(x - h, y, z)$. Using the above definitions, we get

$$E(x - h, y, 0) = a'_{00}U_{00}(x - h, y, 0) = a'_{00}\widetilde{C}e^{-\left((x-h)^2+y^2\right)/w_0^2}, \tag{43}$$

where $\widetilde{C}$ is a complex constant that includes the factors common to all $U_{mn}$. The problem now is to write this as a sum of eigenmodes, $U_{mn}(x, y, 0)$. Let us define $\hat{x} = h/w_0$; if $\hat{x} \ll 1$, we have

$$a'_{00}\widetilde{C}e^{-y^2/w_0^2}e^{-\left((x-h)^2\right)/w_0^2} = a'_{00}\widetilde{C}e^{-\left(x^2+y^2\right)/w_0^2}e^{\left(2xh-h^2\right)/w_0^2}$$

$$a'_{00}U_{00}\exp\left(\left(\frac{2x}{w_0}\right)\hat{x} - \hat{x}^2\right) \approx a'_{00}U_{00}\left[1 + \left(\left(\frac{2x}{w_0}\right)\hat{x} - \hat{x}^2\right) + \frac{1}{2}\left(\left(\frac{2x}{w_0}\right)\hat{x} - \hat{x}^2\right)^2\right], \tag{44}$$

where $U_{00}$ is intended to mean $U_{00}(x, y, 0)$.

Expanding the last line of (44) and discarding terms of higher order than $\hat{x}^2$, we get

$$a'_{00}U_{00}\left[1 + \left(\frac{2x}{w_0}\right) - \hat{x}^2 + \frac{1}{2}\left(\frac{2x}{w_0}\right)^2\hat{x}^2\right]. \tag{45}$$

It is now necessary to write the polynomials in (45) in a manner that facilitates projection onto the orthogonal functions $U_{mn}$. This is most easily done by noting that[14]

$$U_{10} = \left(\frac{2x}{w_0}\right)U_{00} \quad \text{and} \quad U_{20} = \frac{1}{\sqrt{2}}\left(\left(\frac{2x}{w_0}\right)^2 - 1\right)U_{00}. \tag{46}$$

Adding and subtracting $\frac{1}{2}\hat{x}^2$ to (45) yields

$$TEM_{00}(x - h, y, z) = a'_{00}U_{00}\left[\left(1 - \frac{1}{2}\hat{x}^2\right) + \hat{x}\left(\frac{2x}{w_0}\right) + \frac{1}{\sqrt{2}}\hat{x}^2\frac{1}{\sqrt{2}}\left(\left(\frac{2x}{w_0}\right)^2 - 1\right)\right], \tag{47}$$

and using (46) we finally obtain

$$TEM_{00}(x - h, y, z) = \left[a'_{00} \cdot \left(1 - \frac{1}{2}\hat{x}^2\right)\right] \cdot U_{00} + \left[a'_{00} \cdot \hat{x}\right] \cdot U_{10} + \left[a'_{00} \cdot \frac{1}{\sqrt{2}}\hat{x}^2\right] \cdot U_{20}. \tag{48}$$

The expressions in square brackets are exactly the coefficients $a'_{mn}$ that describe the shifted mode in terms of the cavity eigenmodes; this then is the result we desire:

$$\begin{aligned} a_{00} &= a'_{00} \cdot \left(1 - \frac{1}{2}\hat{x}^2\right) \\ a_{10} &= a'_{00} \cdot \hat{x} \\ a_{20} &= a'_{00} \cdot \frac{1}{\sqrt{2}}\hat{x}^2, \quad \text{and} \\ a_{mn} &\approx 0 \cdot a'_{00} \quad \{m > 2 \quad \text{or} \quad n \neq 0\}. \end{aligned} \tag{49}$$

Clearly, the process used above was cumbersome and inefficient. This point becomes painfully obvious when we consider the fact that we made the only non-zero field the $TEM_{00}$. In fact, if there had been a component of $TEM_{10}$, it would make a significant contribution to all $a_{mn}$. One must start with

---

[14]These next equations are straightforward to derive using (40) and (42).

$E = a'_{00}U_{00} + a'_{10}U_{10} + a'_{01}U_{01}$, replace all instances of $x$ by $(x - h)$, expand, and project. This is a terrible way to do things.

Two orthonormality conditions simplify the process above

$$\int\limits_{-\infty}^{\infty} \overline{u_k(x, z)} u_l(x, z) \, \mathrm{d}x \;=\; \delta_{kl} \quad \text{and}$$

$$\int\limits_{-\infty}^{\infty} \int\limits_{-\infty}^{\infty} \overline{U_{mn}(x, y, z)} U_{kl}(x, y, z) \, \mathrm{d}x \, \mathrm{d}y \;=\; \delta_{mk} \delta_{nl} \,. \tag{50}$$

If the original electric field were some arbitrary function $f(x, y, z)$, we could express it as a sum of $U_{mn}(x, y, z)$ in the basis of the unperturbed cavity:

$$f(x, y, z) = \sum_{m,n} a_{mn} \cdot U_{mn} \,. \tag{51}$$

Using (50) and Fourier's trick, one easily obtains

$$a_{mn} = \int\limits_{-\infty}^{\infty} \int\limits_{-\infty}^{\infty} \overline{U_{mn}(x, y, z)} f(x, y, z) \, \mathrm{d}x \, \mathrm{d}y \,. \tag{52}$$

This then replaces all the work done from (43) to (49).

It is usually the case that the input field is the sum of perturbed $U_{kl}$; let us write this as

$$f(x, y, z) = Op\left[E(x, y, z)\right] = \sum_{k,l} a'_{kl} Op\left[U_{kl}(x, y, z)\right] \,. \tag{53}$$

For instance, in the above example, the operator $Offset[E(x, y, z)] = E(x - h, y, z)$. Inserting this into (52),

$$a_{mn} = \sum_{k,l} a'_{kl} \int\limits_{-\infty}^{\infty} \int\limits_{-\infty}^{\infty} \overline{U_{mn}(x, y, z)} Op\left[U_{kl}(x, y, z)\right] \, \mathrm{d}x \, \mathrm{d}y \,. \tag{54}$$

With the stipulation that we are working with dual-indexed vector elements, (54) has the flavor of a linear operator acting on a vector. In fact, this is exactly what one means by the modal model, and the vector space is called modal space. If we define

$$M^{Op}_{mn,kl} = \int\limits_{-\infty}^{\infty} \int\limits_{-\infty}^{\infty} \overline{U_{mn}(x, y, z)} Op\left[U_{kl}(x, y, z)\right] \, \mathrm{d}x \, \mathrm{d}y \,, \tag{55}$$

then (54) becomes simply

$$a_{mn} = \sum_{k,l} a'_{kl} M^{Op}_{mn,kl} \,. \tag{56}$$

Although this can obviously be generalized, we will be primarily concerned with only three fields: TEM$_{00}$, TEM$_{10}$, and TEM$_{01}$. In this case, $M^{Op}_{mn,kl}$ is made up of nine elements. If we define the electric field at any point in space to be

$$E = a_{00}\mathbf{U}_{00} + a_{10}\mathbf{U}_{10} + a_{01}\mathbf{U}_{01} = \begin{bmatrix} a_{00} \\ a_{10} \\ a_{01} \end{bmatrix} \,, \tag{57}$$

then the nine elements of $M_{mn,kl}^{Op}$ can be arrayed in a 3x3 matrix as

$$M^{Op} = \begin{bmatrix} M_{00,00} & M_{10,00} & M_{01,00} \\ M_{00,10} & M_{10,10} & M_{01,10} \\ M_{00,01} & M_{10,01} & M_{01,01} \end{bmatrix}, \tag{58}$$

where the first and second pairs of indices are for the outgoing and incoming fields, respectively. In other words, $M_{01,00}$ would be the ratio of unperturbed $TEM_{01}$ produced to the amount of $Op[TEM_{00}]$ incident. Obviously, the ratio depends on the specific form of the operator.

If one performs the multiplication

$$\begin{bmatrix} M_{00,00} & M_{10,00} & M_{01,00} \\ M_{00,10} & M_{10,10} & M_{01,10} \\ M_{00,01} & M_{10,01} & M_{01,01} \end{bmatrix} \begin{bmatrix} a_{00} \\ a_{10} \\ a_{01} \end{bmatrix} = \begin{bmatrix} M_{00,00}a_{00} + M_{10,00}a_{10} + M_{01,00}a_{01} \\ M_{00,10}a_{00} + M_{10,10}a_{10} + M_{01,10}a_{01} \\ M_{00,01}a_{00} + M_{10,01}a_{10} + M_{01,01}a_{01} \end{bmatrix}, \tag{59}$$

one can see that the matrix only deals with $TEM_{00}$, $TEM_{10}$, and $TEM_{01}$. It gives the amplitudes of the outgoing modes as a function of the amplitudes of the incoming modes and the type of perturbation.

The next four sections will give the details of four different coupling operators: offset, tilt, mismatch of beam waist size, and mismatch of beam waist position.

### 4.2.4   Offset Coupling
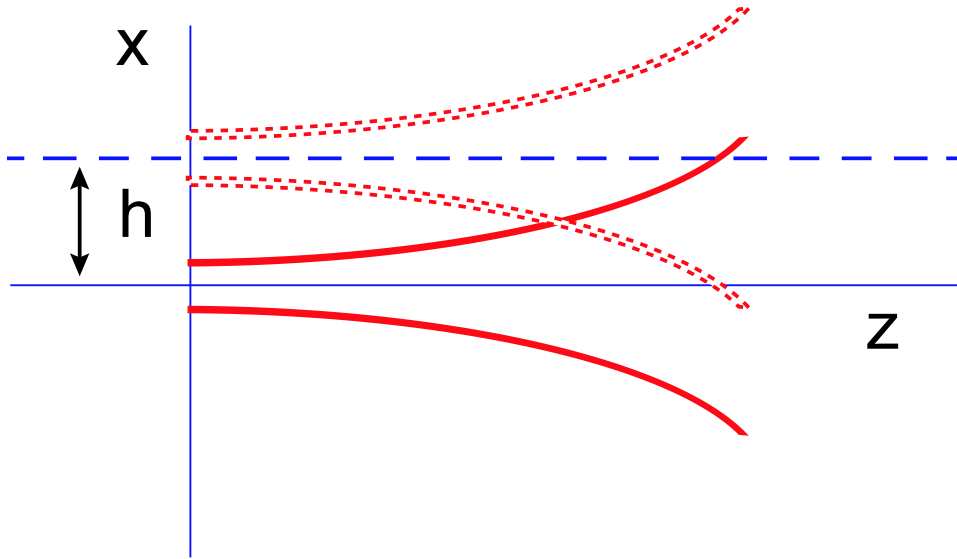


Figure 9: The input beam (dashed) is offset by $h$ in the $x$ direction with respect to the cavity eigenmode (solid).

In its full generality, an offset mode is displaced both in the x and y directions; an offset in the x direction is illustrated in Figure 9[15]. Let us define the offset operator as

$$Offset[E(x,y,z)] = E(x-h,y-k,z). \tag{60}$$

---

[15]Figures 9, 10, 11, 12, 13, and 14 in this section have been adapted from [6] with permission.

Thus, using (55),

$$M_{mn,kl}^{Offset} = \int\limits_{-\infty}^{\infty} \int\limits_{-\infty}^{\infty} \overline{U_{mn}(x,y,z)} U_{kl}(x-h, y-k, z)\, \mathrm{d}x\, \mathrm{d}y, . \tag{61}$$

Since an offset mode stays offset by the same amount as it propagates, we can choose to do the decomposition anywhere we want; for simplicity, let us choose the plane $z = 0$. Just as in the worked example, we define $\hat{x} = h/w_0$ and $\hat{y} = k/w_0$. Evaluating (61) by straightforward integration, we get for the matrix,

$$M^{Offset} = \exp\left[-\frac{(\hat{x}^2 + \hat{y}^2)}{2}\right] \begin{bmatrix} 1 & \hat{x} & \hat{y} \\ -\hat{x} & 1 - \hat{x}^2 & -\hat{x}\hat{y} \\ -\hat{y} & -\hat{x}\hat{y} & 1 - \hat{y}^2 \end{bmatrix}. \tag{62}$$

This is the exact answer for these matrix elements, i.e. no approximations have been made as to the smallness of $\hat{x}$ or $\hat{y}$. In practice, the offsets might be on the order of $10\mu$ m at the largest, and the Mode Cleaner beam waist is $1858\mu$ m; so, at most, $\hat{x}$ and $\hat{y}$ are on the order of $5 \times 10^{-3}$. Therefore, it is perfectly sensible to ignore all second order terms; making these approximations, the matrix becomes

$$M^{Offset} \approx \begin{bmatrix} 1 & \hat{x} & \hat{y} \\ -\hat{x} & 1 & 0 \\ -\hat{y} & 0 & 1 \end{bmatrix}. \tag{63}$$

### 4.2.5   Tilt Coupling
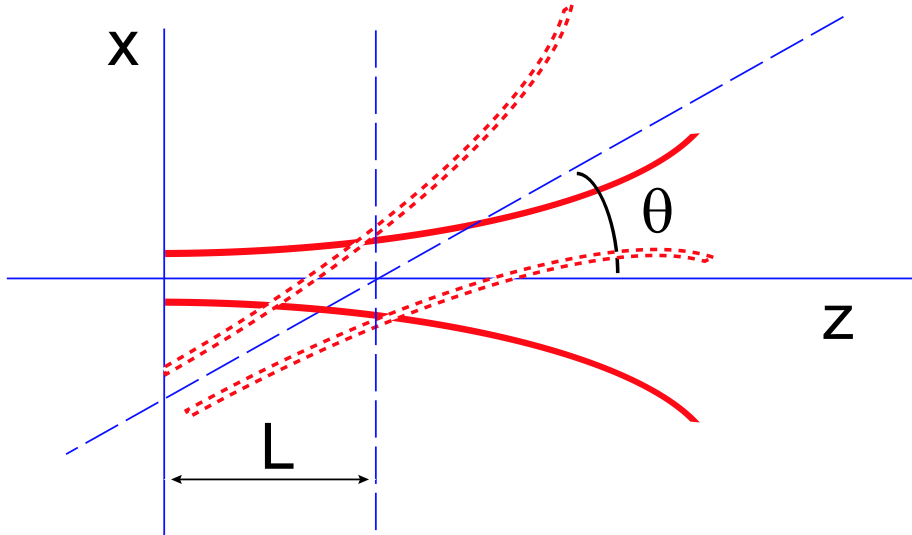


Figure 10: The input beam (dashed) is tilted by $\theta$ with respect to the cavity eigenmode (solid). The axis of rotation is the line parameterized by $\{x = 0, z = L\}$.

Consider a mode tilted with respect to the cavity axis by an amount $\theta_x$ in pitch and $\theta_y$ in yaw, crossing the axis at some arbitrary $z$; this is illustrated in Figure 10. The projection of its amplitude onto the axis will vary as the cosine of the tilt angles; thus, its amplitude does not change to first order. However, the

21

mode will have its bulk phase offset by an amount $\exp\left[-ik\left(\theta_x x + \theta_y y\right)\right]$, where at the crossing point the phase is equal on axis. Therefore, the tilt operator is defined as[16]

$$Tilt[E(x,y,z)] = E(x,y,z)\exp\left[-ik\left(\theta_x x + \theta_y y\right)\right] = E(x,y,z)\exp\left[\frac{-2i\left(\hat{\Theta}_x x + \hat{\Theta}_y y\right)}{w(z)}\right], \quad (64)$$

where

$$\hat{\Theta}_{x(y)} = \theta_{x(y)}\pi w(z)/\lambda = \frac{w(z)}{w_0}\cdot\frac{\theta_{x(y)}}{\theta_D}, \quad (65)$$

and $\theta_D$ is the divergence angle, defined in (17).

So the tilt matrix elements become,

$$M_{mn,kl}^{Tilt} = \int\limits_{-\infty}^{\infty}\int\limits_{-\infty}^{\infty}\overline{U_{mn}(x,y,z)}U_{kl}(x,y,z)\exp\left[\frac{-2i\left(\hat{\Theta}_x x + \hat{\Theta}_y y\right)}{w(z)}\right]\mathrm{d}x\,\mathrm{d}y. \quad (66)$$

Evaluating (66) by straightforward integration,

$$M^{Tilt} = \exp\left[-\frac{\left(\hat{\Theta}_x^2 + \hat{\Theta}_y^2\right)}{2}\right]\begin{bmatrix} 1 & -i\hat{\Theta}_x & -i\hat{\Theta}_y \\ -i\hat{\Theta}_x & 1-\hat{\Theta}_x^2 & -\hat{\Theta}_x\hat{\Theta}_y \\ -i\hat{\Theta}_y & -\hat{\Theta}_x\hat{\Theta}_y & 1-\hat{\Theta}_y^2 \end{bmatrix}. \quad (67)$$

This is the exact answer for these matrix elements, i.e. no approximations have been made as to the smallness of $\hat{\Theta}_x$ or $\hat{\Theta}_y$. In reality, the tilts might be on the order of $10\mu$ rad at the largest, and the Mode Cleaner divergence angle is $182\mu$ rad; so, at most, $\hat{\Theta}_x$ and $\hat{\Theta}_y$ are on the order of $5\times10^{-2}$. Therefore, it is also perfectly sensible to ignore all second order terms in the Tilt matrix; making these approximations, the matrix becomes

$$M^{Tilt} \approx \begin{bmatrix} 1 & -i\hat{\Theta}_x & -i\hat{\Theta}_y \\ -i\hat{\Theta}_x & 1 & 0 \\ -i\hat{\Theta}_y & 0 & 1 \end{bmatrix}. \quad (68)$$

### 4.2.6 Waist Size Mismatch Coupling

The coupling to higher order modes due to the mismatch of the waist size is trivial to compute. The two sets of eigenmodes (those with the correct waist size and those without) are identical in all respects except for the constant $w_0$. If we define the waist of the input beam to be $w_0'$ and that of the cavity eigenmode to be $w_0$, then the operator can be written as

$$WSM[E(x,y,z,w_0)] = E(x,y,z,w_0'), \quad (69)$$

where WSM is an acronym for waist size mismatch.

The WSM matrix elements become,

$$M_{mn,kl}^{WSM} = \int\limits_{-\infty}^{\infty}\int\limits_{-\infty}^{\infty}\overline{U_{mn}(x,y,z,w_0)}U_{kl}(x,y,z,w_0')\,\mathrm{d}x\,\mathrm{d}y. \quad (70)$$

---

[16]In [6], the tilt operator is defined more rigorously as $Tilt\left[E(x,y,z)\right] = E(x\cdot\cos\theta - (z-L)\cdot\sin\theta, y, L + x\cdot\sin\theta + (z-L)\cdot\cos\theta)$, but the answers obtained here will be exactly the same.
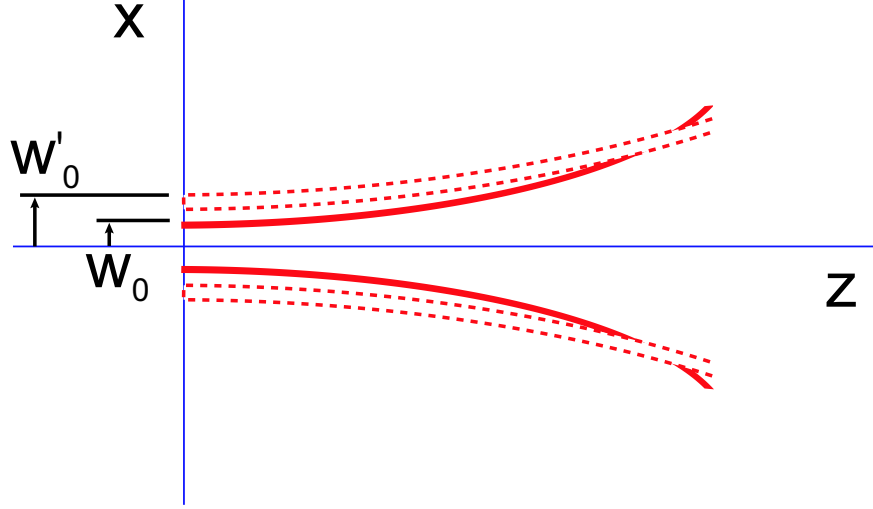
Figure 11: The waist size of the input beam (dashed) is $w_0'$, but the waist size of the cavity eigenmode (solid) is $w_0$.

If we define the coupling coefficient for WSM to be

$$\hat{w} = \frac{w_0'}{w_0} - 1\,,\tag{71}$$

then integrating (70),

$$M^{WSM} = \begin{bmatrix} \dfrac{2\left(\frac{w_0'}{w_0}\right)}{1+\left(\frac{w_0'}{w_0}\right)^2} & 0 & 0 \\[2em] 0 & \left(\dfrac{2\left(\frac{w_0'}{w_0}\right)}{1+\left(\frac{w_0'}{w_0}\right)^2}\right)^2 & 0 \\[2em] 0 & 0 & \left(\dfrac{2\left(\frac{w_0'}{w_0}\right)}{1+\left(\frac{w_0'}{w_0}\right)^2}\right)^2 \end{bmatrix}.\tag{72}$$

This is the exact answer for these matrix elements. If $w' \approx w$, then

$$\frac{2\left(\frac{w_0'}{w_0}\right)}{1+\left(\frac{w_0'}{w_0}\right)^2} \approx 1 - \frac{1}{2}\hat{w}^2\,.\tag{73}$$

This is expression is unity even to first order, and the matrix representing the mismatch will simply be the identity matrix. Therefore, a waist size mismatch will cause no first order coupling.

### 4.2.7 Waist Position Mismatch Coupling

In Figure 12, the waist position of the input beam is offset in the positive direction of propagation. Clearly then, at the origin, the input has a negative and finite radius of curvature. The eigenmode,
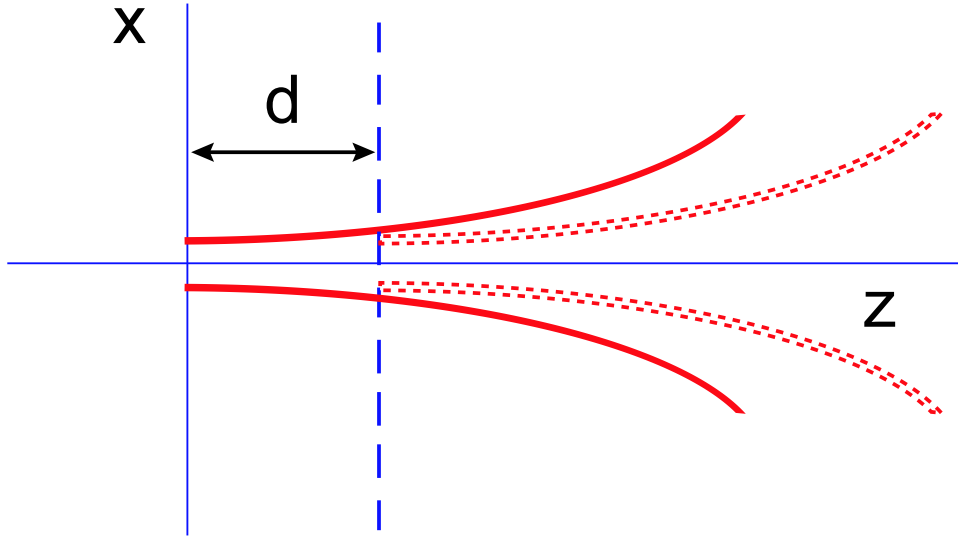
23

Figure 12: The waist of the input beam (dashed) is offset from the waist of the eigenmode (solid) by $d$ in the positive $z$ direction.

however, has an infinite radius of curvature at the origin. To take this into account, we must use the ROC term in (42).

For all $TEM_{mn}$ modes, the transverse phase variation associated with the ROC at a given $z$ is given by

$$\exp\left[\frac{-ik\left(x^2+y^2\right)}{2R(z)}\right].\tag{74}$$

If $d \ll z_0$, then using (12), the ROC becomes approximately

$$R(-d) = -d\left(1+\left(\frac{z_0}{d}\right)^2\right) \approx -\frac{z_0^2}{d}.\tag{75}$$

Substituting (75) into (74) and using (10), we have an approximate expression for the transverse phase

$$\exp\left[-i\frac{2\pi}{\lambda}\left(\frac{-d}{z_0}\right)\frac{1}{2z_0}\left(x^2+y^2\right)\right] = \exp\left[i\,\hat{d}\frac{(x^2+y^2)}{w_0^2}\right],\tag{76}$$

where $\hat{d}=d/z_0$[17].

The operator becomes

$$WPM[E(x,y,-d)] = Prop(-d,0)\cdot\exp\left[i\,\hat{d}\frac{(x^2+y^2)}{w_0^2}\right]E(x,y,0),\tag{77}$$

---

[17]It should be clear that $\hat{d}$ is positive when the input mode has its waist downstream of the eigenmode as shown in Figure 12.

where WPM is an acronym for waist position mismatch, and the propagation operator is defined in (39).

The WPM matrix elements are,

$$M_{mn,kl}^{WPM} = \int\limits_{-\infty}^{\infty} \int\limits_{-\infty}^{\infty} \overline{U_{mn}(x,y,0)} U_{kl}(x,y,-d) Prop(-d,0) \exp\left[i\,\hat{d}\frac{(x^2+y^2)}{w_0^2}\right] \mathrm{d}x\,\mathrm{d}y\,. \qquad (78)$$

Integrating (78),

$$M^{WPM} = \exp[ikd]\cdot\exp[-i(m+n+1)\arctan(d/z_0)] \begin{bmatrix} \frac{1}{1-i\left(\frac{\hat{d}}{2}\right)} & 0 & 0 \\ 0 & \frac{\exp[i2\arctan(\hat{d}/2)]}{1+\left(\frac{\hat{d}}{2}\right)^2} & 0 \\ 0 & 0 & \frac{\exp[i2\arctan(\hat{d}/2)]}{1+\left(\frac{\hat{d}}{2}\right)^2} \end{bmatrix}. \qquad (79)$$

The two exponential factors, $\exp[ikd]$ and $\exp[-i(m+n+1)\arctan(d/z_0)]$, come from bulk displacement and Guoy phase shifts (respectively) acquired from the offset.

Reducing the matrix elements to first order approximations,

$$M^{WPM} \approx \exp[ikd]\cdot\exp[-i(m+n+1)\arctan(d/z_0)] \begin{bmatrix} 1+i\left(\frac{\hat{d}}{2}\right) & 0 & 0 \\ 0 & e^{i\hat{d}} & 0 \\ 0 & 0 & e^{i\hat{d}} \end{bmatrix}. \qquad (80)$$

This can be simplified even further to yield

$$M^{WPM} \approx \exp[-i(m+n+1)\arctan(d/z_0)]\cdot e^{ikd} \begin{bmatrix} e^{i\hat{d}/2} & 0 & 0 \\ 0 & e^{i\hat{d}} & 0 \\ 0 & 0 & e^{i\hat{d}} \end{bmatrix}. \qquad (81)$$

Clearly, there is no change in amplitude associated with WPM, since the magnitude of all the matrix elements are unity to first order. However, the resulting phase shifts will tend to detune the input mode from resonance.

### 4.2.8 The Reflection Operator

In the analysis of cavities, the most significant alignment problem is the tilt in pitch and yaw of the mirrors. In Figures 13 and 14, one can see that when a mirror is tilted away from a beam previously at *normal incidence*, the reflected beam will be travelling at twice the tilt angle with respect to the direction of retroreflection, which is just a statement of the law of reflection. Therefore, one can simply use the tilt operator already discussed in Section 4.2.5 by replacing all instances of $\Theta$ by $2\Theta$.

To determine the sign of $\Theta$, one must compare the direction of propagation of the reflected beam in the new and old coordinate systems [6]. Let us define a front surface reflection to be one in which the beam is travelling in the *negative z* direction and a back surface reflection when travelling in the *positive z* direction. Using Figures 13 and 14 as a guide, one obtains

$$M^{Ref-front} = \begin{bmatrix} 1 & +2i\hat{\Theta}_{pitch} & -2i\hat{\Theta}_{yaw} \\ +2i\hat{\Theta}_{pitch} & 1 & 0 \\ -2i\hat{\Theta}_{yaw} & 0 & 1 \end{bmatrix}, \qquad (82)$$
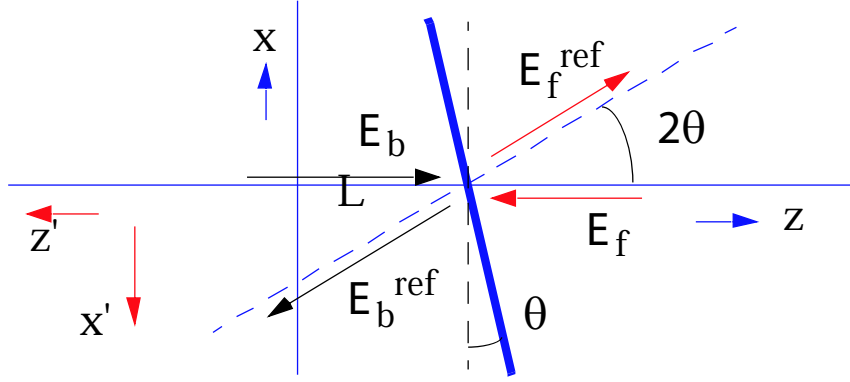
Figure 13: Reflection from the front and back surfaces of a mirror that has been tilted away from normal incidence by $\Theta_y$(yaw).
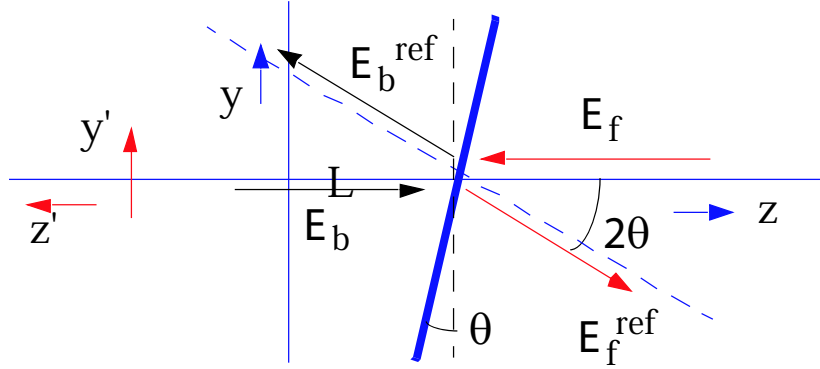


Figure 14: Reflection from the front and back surfaces of a mirror that has been tilted away from normal incidence by $\Theta_x$(pitch).

for reflections off the front surface at normal incidence, and

$$M^{Ref-back} = \begin{bmatrix} 1 & -2i\hat{\Theta}_{pitch} & -2i\hat{\Theta}_{yaw} \\ -2i\hat{\Theta}_{pitch} & 1 & 0 \\ -2i\hat{\Theta}_{yaw} & 0 & 1 \end{bmatrix}, \tag{83}$$

for reflections off the back surface at normal incidence.

Keep in mind that if the mirror is defined to be aligned when it is not at normal incidence (in a ring cavity, for example), then the beam will not necessarily be deflected through twice the tilt angle of the mirror.

Figure 15 illustrates reflection from a mirror. The vector law of reflection gives the wavevector, $\mathbf{k}'$, of reflected rays in terms of the incident ray's wavevector, $\mathbf{k}$. If the mirror's surface has unit-normal vector $\hat{\mathbf{n}}$ at the point of reflection, then

$$\mathbf{k}' = \mathbf{k} - 2(\hat{\mathbf{n}} \cdot \mathbf{k})\hat{\mathbf{n}}. \tag{84}$$

One would like to parameterize the deflection of the reflected ray in terms of small misalignments of the mirror. The rotation matrices for yaw and pitch are
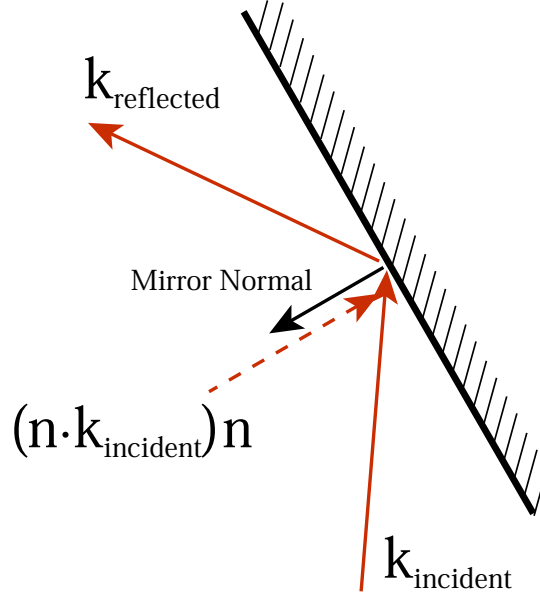
Figure 15: The vector law of reflection says that the **k**-vector's projection onto the mirror normal changes sign on reflection.

$$R^{yaw} = \begin{bmatrix} \cos y & \sin y & 0 \\ -\sin y & \cos y & 0 \\ 0 & 0 & 1 \end{bmatrix} \quad \text{and} \quad R^{pitch} = \begin{bmatrix} 1 & 0 & 0 \\ 0 & \cos p & \sin p \\ 0 & -\sin p & \cos p \end{bmatrix}, \tag{85}$$

where p and y are the pitch and yaw angles respectively. If the angles are small, then the matrices become

$$R^{yaw} \approx \begin{bmatrix} 1 & y & 0 \\ -y & 1 & 0 \\ 0 & 0 & 1 \end{bmatrix} \quad \text{and} \quad R^{pitch} \approx \begin{bmatrix} 1 & 0 & 0 \\ 0 & 1 & p \\ 0 & -p & 1 \end{bmatrix}. \tag{86}$$

These two matrices in their approximate form commute with each other; in addition, they are incremental in the sense that one could move one degree in both pitch and yaw by making 10, 0.1 degree steps in any order.

In this context, the pitch and yaw angles form a coordinate pair and define a unique orientation for the mirror. If the initial normal vector of the mirror is described in terms of the spherical coordinate angles, $\theta$ and $\phi$, then the aligned normal vector will be

$$\hat{\mathbf{n}} = \begin{bmatrix} \sin\theta\cos\phi \\ \sin\theta\sin\phi \\ \cos\theta \end{bmatrix}. \tag{87}$$

Applying the inverse of the reflection operators[18] from equation (85),

$$\hat{\mathbf{n}}' = \begin{bmatrix} \sin\theta\cos\phi - y\cdot\sin\theta\sin\phi \\ y\cdot\sin\theta\cos\phi + \sin\theta\sin\phi - p\cdot\cos\theta \\ p\cdot\sin\theta\sin\phi + \cos\theta \end{bmatrix}. \tag{88}$$

---

[18]The inverse matrices are used because one wants to describe the misaligned system *from the aligned system*.

27

One can now use the normal vector in (88) with (84) to determine how much the reflected beam will be deflected from its aligned direction for a given misalignment in pitch or yaw.

### 4.2.9 Propagation Matrix

When TEM$_{mn}$ modes propagate from point 1 to point 2, a unit of Guoy phase is defined to be

$$Prop(z_2, 0) - Prop(z_1, 0) = e^{-ik(z_2-z_1)} \left( \arctan\left[\frac{z_2}{z_0}\right] - \arctan\left[\frac{z_1}{z_0}\right] \right) = e^{-ik(z_2-z_1)}\Delta\eta \qquad (89)$$

In terms of the matrix algebra then, we can define a propagation matrix

$$Prop(z_2, z_1) = e^{-ik(z_2-z_1)} \begin{bmatrix} e^{i\Delta\eta} & 0 & 0 \\ 0 & e^{2i\Delta\eta} & 0 \\ 0 & 0 & e^{2i\Delta\eta} \end{bmatrix}. \qquad (90)$$

### 4.2.10 Unitary Property of the Reflection Operator

An important property of the reflection operator is that it is unitary to first order in $\hat{\Theta}$:

$$MM^{\dagger} = \begin{bmatrix} 1 & ci\hat{\Theta}_1 & di\hat{\Theta}_2 \\ ci\hat{\Theta}_1 & 1 & 0 \\ di\hat{\Theta}_2 & 0 & 1 \end{bmatrix} \begin{bmatrix} 1 & -ci\hat{\Theta}_1 & -di\hat{\Theta}_2 \\ -ci\hat{\Theta}_1 & 1 & 0 \\ -di\hat{\Theta}_2 & 0 & 1 \end{bmatrix} \qquad (91)$$

$$= \begin{bmatrix} 1 + (c\Theta_1)^2 + (d\Theta_2)^2 & -ci\hat{\Theta}_1 + ci\hat{\Theta}_1 & -di\hat{\Theta}_2 + di\hat{\Theta}_2 \\ -ci\hat{\Theta}_1 + ci\hat{\Theta}_1 & 1 + (c\Theta_1)^2 & cd\Theta_1\Theta_2 \\ -di\hat{\Theta}_2 + di\hat{\Theta}_2 & cd\Theta_1\Theta_2 & 1 + (d\Theta_1)^2 \end{bmatrix} \qquad (92)$$

$$\approx \begin{bmatrix} 1 & 0 & 0 \\ 0 & 1 & 0 \\ 0 & 0 & 1 \end{bmatrix}. \qquad (93)$$

Here, $c$ and $d$ are real coefficients that give the amount of coupling ($c = d = 2$ for reflections at normal incidence).

The unitary property will be used often in the calculation of misaligned cavity fields because inversion of a reflection matrix is identical to conjugation and transposition, which are much simpler operations.

## 4.3 Misaligned Optical Cavities

The steady-state fields of optical cavities are normally deduced under the assumption that the cavity is perfectly aligned. Normally, deducing the fields of a *misaligned* cavity would involve finding solutions to Maxwell's equations that satisfied the perturbed boundary conditions. However, with the methods discussed in Section 4.2, we can easily find the fields in misaligned optical cavities.
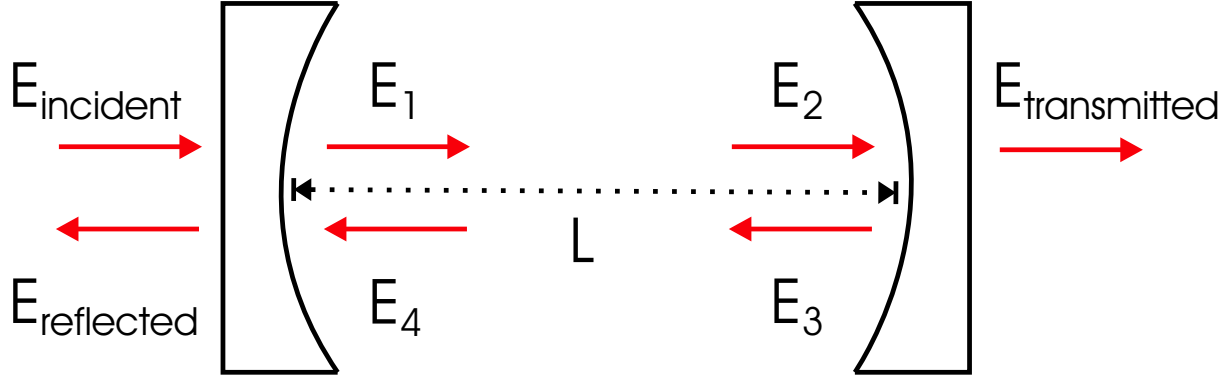
Figure 16: A typical Fabry-Perot cavity is constructed of two partially reflecting mirrors, separated by a distance, L. The left-travelling and right-travelling waves are the steady-state fields of the cavity.

### 4.3.1 Worked example: The Fabry-Perot Interferometer

Consider the simple case of a perfectly-aligned Fabry-Perot cavity. If the incident field is matched to the cavity's eigenmode, then all the fields in Figure 16 will have the same spatial properties as the incident field. We can therefore deal only with the amplitudes and phases of the fields as there will be no coupling between different transverse modes.

We would like to write the transmitted, reflected, and circulating fields in terms of the input field. The easiest way to do this is to find a set of fields that are self-consistent:

$$E_{reflected} = r_1 E_{incident} + t_1 E_4 \tag{94}$$
$$E_{transmitted} = t_2 E_2 \tag{95}$$
$$E_1 = t_1 E_{incident} - r_1 E_4 \tag{96}$$
$$E_2 = e^{i\phi} E_1 \tag{97}$$
$$E_3 = -r_2 E_2 \tag{98}$$
$$E_4 = e^{i\phi} E_3, \tag{99}$$

where $e^{i\phi} = Prop(L/2, -L/2)$ as defined in (39). The reflectivities and transmissivities satisfy the relations

$$r_i = \sqrt{R_i} \tag{100}$$
$$t_i = \sqrt{T_i} \tag{101}$$
$$R + T + L = 1, \tag{102}$$

where L is the relative energy loss per pass.

The convention has been used here that a phase shift of $\pi$ (sign flip) is added for reflections off coated sides of mirrors[19].

Equations (96) through (99) yield a solution for $E_1$:

$$E_1 \equiv E_{circulating} = t_1 E_{incident} + r_1 r_2 e^{2i\phi} E_{circulating} = \frac{t_1}{1 - r_1 r_2 e^{2i\phi}} E_{incident}. \tag{103}$$

---

[19]In this case the curved faces of the mirrors are taken to be coated

This circulating field is related to all the fields internal to the cavity by a multiplicative constant using (96) through (99). In particular,

$$E_2 = e^{i\phi}E_{circulating} \tag{104}$$

$$E_4 = -r_2 e^{2i\phi}E_{circulating}. \tag{105}$$

Substituting (103) through (105) into (94) and (95) yields

$$E_{reflected} = \left(r_1 - \frac{r_2 t_1^2 e^{2i\phi}}{1 - r_1 r_2 e^{2i\phi}}\right)E_{incident} \tag{106}$$

$$E_{transmitted} = \frac{t_1 t_2 e^{i\phi}}{1 - r_1 r_2 e^{2i\phi}}E_{incident}. \tag{107}$$

Equations (103, (106), and (107) determine all the fields in Figure 16. Any standard optics text[20] will discuss these field equations in full detail.

Let us write the fields in a slightly different form:

$$E_{circulating} = t_1[1 - r_1 r_2 G_{rt}]^{-1}E_{incident} \tag{108}$$

$$E_{reflected} = [r_1 - (r_1^2 + t_1^2)r_2 G_{rt}][1 - r_1 r_2 G_{rt}]^{-1}E_{incident} \tag{109}$$

$$E_{transmitted} = t_1 t_2 Prop(L/2, -L/2)[1 - r_1 r_2 G_{rt}]^{-1}E_{incident}, \tag{110}$$

where $G_{rt}$ is the round trip operator that transforms the field $E_1$ into the field $E_4$[21]. In this case,

$$G_{rt} = Prop(L/2, -L/2)Prop(L/2, -L/2). \tag{111}$$

If the cavity were misaligned, then at each reflection, there could also be a change in amplitude or phase due to coupling between different TEM$_{mn}$ modes. The amount of coupling is given by the operators defined in Section 4.2. Equations (94) through (99) become

$$E_{reflected} = r_1 \mathbf{M}_1 E_{incident} + \mathbf{I}t_1 E_4 \tag{112}$$

$$E_{transmitted} = t_2 \mathbf{I}E_2 \tag{113}$$

$$E_1 = t_1 \mathbf{I}E_{incident} - r_1 \mathbf{M}_1 E_4 \tag{114}$$

$$E_2 = \mathbf{Prop(L/2,-L/2)}E_1 \tag{115}$$

$$E_3 = -r_2 \mathbf{M}_2 E_2 \tag{116}$$

$$E_4 = \mathbf{Prop(L/2,-L/2)}E_3, \tag{117}$$

Here, the fields are vectors whose elements contain the amplitude and phase of each TEM$_{mn}$ mode[22]. These equations will be solved in exactly the same way as above; however, instead of division, the equations must be manipulated using matrix inversion[23].

---

[20] See for instance [7], section 9.6.

[21] The definitions of these fields are shown in Figure 16.

[22] This was described on page 19, (57).

[23] Note that $\mathbf{I}$ is the identity matrix.

$$E_{circulating} = t_1[\mathbf{I} - r_1 r_2 \mathbf{G}_{rt}]^{-1} E_{incident} \tag{118}$$

$$E_{reflected} = \mathbf{M}_1^\dagger [\mathbf{I}r_1 - (r_1^2 + t_1^2)r_2 \mathbf{G}_{rt}][\mathbf{I} - r_1 r_2 \mathbf{G}_{rt}]^{-1} E_{incident} \tag{119}$$

$$E_{transmitted} = t_1 t_2 \mathbf{Prop}_{1\to2}[\mathbf{I} - r_1 r_2 \mathbf{G}_{rt}]^{-1} E_{incident} \tag{120}$$

$$\mathbf{G}_{rt} = \mathbf{M}_1 \mathbf{Prop}_{2\to1} \mathbf{M}_2 \mathbf{Prop}_{1\to2} \tag{121}$$

One can now easily deduce the amplitudes and phases of the $\mathrm{TEM}_{00}$, $\mathrm{TEM}_{10}$, and $\mathrm{TEM}_{01}$ fields at any point in space. We will be particularly interested in the reflected field.
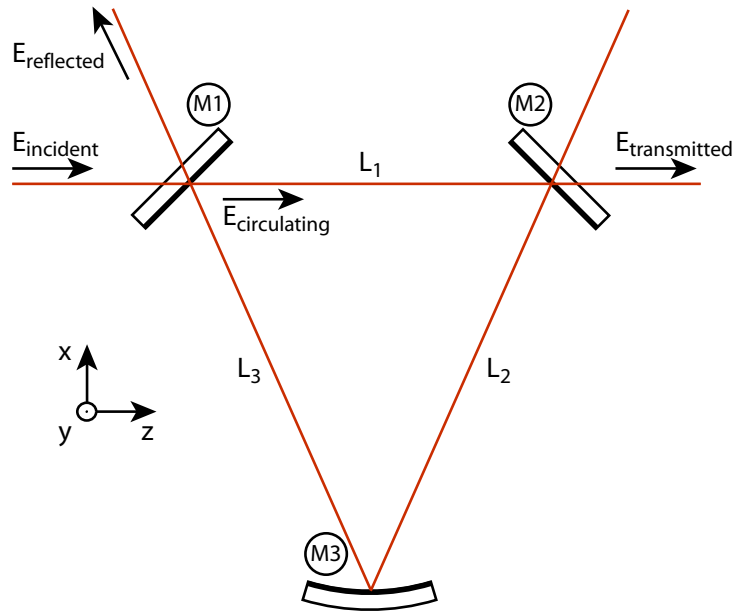
### 4.3.2 The Triangular Mode-Cleaner Cavity



Figure 17: LIGO mode cleaners are triangular; there are typically two flat mirrors placed close together and a third, curved mirror placed far from the other two.

Figure 17 shows a schematic diagram of a triangular mode cleaner cavity. All conventions used in this analysis will be those used in [8].

The two flat mirrors, $\mathrm{M}_1$ and $\mathrm{M}_2$, are set at $\pm45$ degrees from the $z$ axis; thus, $L_2 = L_3$, and the cavity has a line of symmetry that runs parallel to the x axis, halfway between the two flat mirrors.

The spatial properties of the beam can be found using the resonator algebra defined in Section 4.1.5. Since the cavity waist, by symmetry, occurs halfway between the two flat mirrors, the triangular cavity is equivalent to a symmetric Fabry-Perot cavity with half-length $L \equiv L_1/2 + L_2 = L_1/2 + L_3$, and both mirrors having a radius of curvature $R$, equal to that of the triangular cavity's curved mirror. Thus,

$$z_0 = \sqrt{L(R - L)}. \tag{122}$$

To derive the cavity fields shown in Figure 17, one does exactly the same analysis as that shown in Section 4.3.1. There is one quirk in the derivation that must be mentioned: because of the odd number

of reflections, there is a spatial flip that occurs for fields in the $x - z$ plane. This can be described with a "flip-in-x" operator [8] defined as

$$X_{mn,kl} = (-1)^m \delta_{mk} \delta_{nl} \Leftrightarrow X = \begin{bmatrix} 1 & 0 & 0 \\ 0 & -1 & 0 \\ 0 & 0 & 1 \end{bmatrix} . \tag{123}$$

This operator must act on the fields each each time they circulate in the cavity.

The field equations become

$$
\begin{align}
E_{circulating} &= t_1 [\mathbf{I} - r_1 r_2 r_3 \mathbf{G}_{rt}]^{-1} E_{incident} \tag{124} \\
E_{reflected} &= \mathbf{M}_1 [\mathbf{I} r_1 - (r_1^2 + t_1^2) r_2 r_3 \mathbf{G}_{rt}][\mathbf{I} - r_1 r_2 r_3 \mathbf{G}_{rt}]^{-1} E_{incident} \tag{125} \\
E_{transmitted} &= t_1 t_2 \mathbf{Prop}_{L_1} [\mathbf{I} - r_1 r_2 r_3 \mathbf{G}_{rt}]^{-1} E_{incident} \tag{126} \\
\mathbf{G}_{rt} &= -\mathbf{X} \mathbf{M}_1{}^\dagger \mathbf{Prop}_{L_3} \mathbf{M}_3{}^\dagger \mathbf{Prop}_{L_2} \mathbf{M}_2{}^\dagger \mathbf{Prop}_{L_1} \tag{127}
\end{align}
$$

## 4.4 Modulation, Demodulation, and Control

Section 4.3 describes how the fields of an interferometer are transformed when an optical cavity is misaligned. In this section, we will show how a laser with two phase modulation sidebands can be used to produce an error signal that is proportional to a specific cavity misalignment such as the tilt of a front mirror.

### 4.4.1 Motivation

Consider a sine-phase modulated laser reflected from a Fabry-Perot Cavity[24]. When the carrier is resonant, it will be completely *transmitted*, but the sidebands, which are far from resonance, are completely *reflected*. If, however, the back mirror is misaligned in the x-z plane, then a small amount of $\text{TEM}_{10}$ at the carrier frequency will be reflected as well. The sidebands are unaffected by this misalignment because they do not resonate inside the cavity.

This is simply modelled[25] as

$$
\begin{align}
E(x, y, t) &= iTEM_{00}[\omega - \Omega] - iTEM_{00}[\omega + \Omega] + ae^{i\theta} TEM_{10}[\omega] \tag{128} \\
&\propto e^{-(x^2 + y^2)} \left[ ie^{i(\omega - \Omega)t} - ie^{i(\omega + \Omega)t} + ae^{i\theta} e^{i\omega t} 2x \right] , \tag{129}
\end{align}
$$

where $\theta$ is the relative (Guoy) phase of the reflected $\text{TEM}_{10}$ and $\text{TEM}_{00}$ modes, and a is a real constant that describes the amount the mirror is misaligned.

The intensity falling on the photodiode is proportional to the absolute square of the field:

$$
\begin{align}
I(x, y, t) &\propto E(x, y, t) \overline{E(x, y, t)} \tag{130} \\
&\propto e^{-2(x^2 + y^2)} \left[ 2 - 2\cos[2\Omega t] + (2ax)^2 + 8ax \sin[\Omega t] \cos[\theta] \right] . \tag{131}
\end{align}
$$

To see what this means, let us examine the behavior of the intensity for $a = 0.5$ and various values of $\theta$, which can be varied by letting the fields propagate in space because the $\text{TEM}_{10}$ will advance twice as fast as the $\text{TEM}_{00}$ fields.

---

[24]The meaning of phase modulation will be made clear in the following section.

[25]The specific form of the field should become absolutely clear in the following sections.

For $\theta = 0$, $\pi/4$, $\pi/2$, we get

$$I(x, y, t)_{\theta=0} = e^{-2(x^2+y^2)} \left[ 2 - 2\cos[2\Omega t] + (2ax)^2 + 8ax\sin[\Omega t] \right], \tag{132}$$

$$I(x, y, t)_{\theta=\pi/4} = e^{-2(x^2+y^2)} \left[ 2 - 2\cos[2\Omega t] + (2ax)^2 + (8/\sqrt{2})ax\sin[\Omega t] \right], \tag{133}$$

$$I(x, y, t)_{\theta=\pi/2} = e^{-2(x^2+y^2)} \left[ 2 - 2\cos[2\Omega t] + (2ax)^2 \right]. \tag{134}$$

Figures 18, 19, and 20 show these intensity distributions at different snapshots in time.



Figure 18: When $\theta = 0$, a thick line appears to move through the spot with frequency $\Omega$. This series extends over a time interval equal to $1/\Omega$.



Figure 19: When $\theta = \pi/4$, one spot gets smaller than and swallowed by the other at frequency $\Omega$. This series also extends over a time interval equal to $1/\Omega$.

Figures 18, 19, and 20 show the time varying intensity distributions given by the above three equations. The important thing to notice about these figures is that, although there will be a time-varying intensity pattern for all values of $\theta$, the symmetry of that distribution varies with $\theta$ as well. Let us try to

Figure 20: When $\theta = \pi/2$, the two spots symmetrically merge together at frequency $2\Omega$, and nothing happens at frequency $\Omega$. This series extends over a time interval equal to $1/2\Omega$ because nothing is happening at frequency $\Omega$.

parameterize this symmetry property by finding the difference in total intensity on the left and right side of $x = 0$. We will call this function Err:

$$\text{Err}(t) = \int_0^\infty \int_{-\infty}^\infty I(x, y, t) \, \mathrm{d}y \mathrm{d}x - \int_{-\infty}^0 \int_{-\infty}^\infty I(x, y, t) \, \mathrm{d}y \mathrm{d}x \tag{135}$$

If one looks at (131), it is clear that the only term that is not symmetric with respect to $x = 0$ is the term $e^{-2(x^2+y^2)} 8ax \sin[\Omega t] \cos[\theta]$. Therefore, all the other terms do not contribute to Err, and the value of Err becomes

$$\text{Err}(t) = \sqrt{8\pi} a \cos[\theta] \sin[\Omega t] \,. \tag{136}$$

We now have an error signal that is proportional to the amplitude and sensitive to the relative phase of the $\text{TEM}_{10}$ mode incident on the detector. This error signal oscillates sinusoidally at $\Omega$, and if we multiply by $\sin[\Omega t]$ and average over one cycle (I-phase demodulation), we obtain a constant error signal that is proportional to the misalignment, a.

If we were to use a detector constructed of two half-planes (left and right of $x = 0$), then we could subtract the signals from these two halves to generate $\text{Err}(t)$, and then use demodulation to reduce $\text{Err}(t)$ to a constant error signal.

Referring back to Section 4.2.1, we know that if the mirror is offset, $\theta = 0$, and we should place a photodiode as close as possible to the cavity because we are most sensitive when $\theta = 0$; we would then have an error signal proportional to the offset.

If the mirror is tilted, then $\theta = \pi/2$, and we have no sensitivity to tilt; however, if we allow the fields to propagate into the far-field, then $\theta$ will evolve to 0 again, and we will have an error signal proportional to the tilt.

This is *amazing*! We have an error signal where we can optically determine what sort of misalignment we can see. If we want offset, we have a near-field photodiode; if we want tilt, we have a far-field photodiode, and each is blind to the other.

If this weren't enough, if we had also allowed the front mirror to be misaligned, then

$$E(x, y, t) \;=\; (iTEM_{00}[\omega - \Omega] - iTEM_{00}[\omega + \Omega])(1 + be^{i\alpha}) + ae^{i\theta}TEM_{10}[\omega] \tag{137}$$

34

$$\propto \quad e^{-(x^2+y^2)}\left[(ie^{i(\omega-\Omega)t} - ie^{i(\omega+\Omega)t})(1 + be^{i\alpha}) + ae^{i\theta}e^{i\omega t}2x\right], \tag{138}$$

Going through the same simple procedure, we would find

$$\text{Err}(t) = \sqrt{8\pi}(a\cos[\theta]\sin[\Omega t] - b\cos[\alpha]\cos[\Omega t] + b\cos[\alpha]). \tag{139}$$

If we multiply by $\sin[\Omega t]$ and average over a cycle, we get

$$\text{Err} \propto a\cos[\theta]. \tag{140}$$

If we multiply by $\cos[\Omega t]$ and average over a cycle, we get

$$\text{Err} \propto b\cos[\alpha]. \tag{141}$$

Thus, by picking the demodulation phase[26], we can choose which mirror we are sensitive to (I-phase for the front mirror and Q-phase for the back), and then we can pick the kind of misalignment we want to see by controlling the propagation distance.

The beauty and simplicity of this scheme accounts for its ubiquity.

### 4.4.2 Phase Modulation

If the phase of an electric field is sinusoidally modulated in time, it can be decomposed into three fields with a well-defined relationship:

$$e^{i\omega t} \quad \Rightarrow \quad e^{i(\omega t + \Gamma\sin\Omega t)} \approx e^{i\omega t}\left(1 + i\Gamma\sin\Omega t\right) \tag{142}$$

$$= \quad e^{i\omega t}\left(1 + \frac{\Gamma}{2}e^{i\Omega t} - \frac{\Gamma}{2}e^{-i\Omega t}\right) = e^{i\omega t} + \frac{\Gamma}{2}e^{i(\omega+\Omega)t} - \frac{\Gamma}{2}e^{i(\omega-\Omega)t}, \tag{143}$$

where $\Gamma$ is a small number called the modulation index.

Clearly, the modulated phase decomposes into the original field, one field shifted up by the modulation frequency, and one field shifted down by the modulation frequency.

### 4.4.3 Demodulation

If a phase modulated field is incident on a photodiode, the intensity measured will be

$$E\overline{E} \quad = \quad (E_0 + E_+e^{i\Omega t} + E_-e^{-i\Omega t})e^{i\omega t}(\overline{E_0} + \overline{E_+}e^{-i\Omega t} + \overline{E_-}e^{+i\Omega t})e^{-i\omega t} \tag{144}$$

$$= \quad [|E_0|^2 + |E_+|^2 + |E_-|^2] + [(E_0\overline{E_-} + E_+\overline{E_0})e^{i\Omega t}) + CC] + [E_+\overline{E_-}e^{2i\Omega t}) + CC] \tag{145}$$

If one multiplies this intensity by $\cos(\Omega t + \phi)$ and averages over one cycle, then only the terms oscillating at $\Omega$ will have a non-zero average. If we define this demodulated signal to be $S$, then

$$S = \frac{\Omega}{2\pi}\int_t^{t+\frac{2\pi}{\Omega}}\left(A\cos(\Omega\tau + \phi)e^{i\Omega\tau} + \overline{A}\cos(\Omega\tau + \phi)e^{-i\Omega\tau}\right)d\tau, \tag{146}$$

where

$$A = E_0\overline{E_-} + E_+\overline{E_0}. \tag{147}$$

[26]This is explained below.

This is a simple integration to perform:

$$S = \frac{1}{2}\left(Ae^{-i\phi} + \overline{A}e^{i\phi}\right). \tag{148}$$

$\phi$ is known as the demodulation phase, and from (148) we can recover the well-known results:

$$\phi = 0 \quad \Rightarrow \quad \cos(\Omega t + \phi) = \cos(\Omega t) \tag{149}$$

$$S = S_I = Re[A] = Re[E_0\overline{E_-} + E_+\overline{E_0}] \tag{150}$$

$$\phi = -\frac{\pi}{2} \quad \Rightarrow \quad \cos(\Omega t + \phi) = \cos(\Omega t) \tag{151}$$

$$S = S_Q = -Im[A] = -Im[E_0\overline{E_-} + E_+\overline{E_0}]. \tag{152}$$

Note, however, that $\phi$ can take on any value.

### 4.4.4 Demodulation with Higher Order Modes Present

In the model, we will need to take into account the different spatial components of fields. Suppose we substitute into (144)

$$E_0 = A^c\psi_{00} + B^c\psi_{10} + C^c\psi_{01} \tag{153}$$

$$E_+ = A^+\psi_{00} + B^+\psi_{10} + C^+\psi_{01} \tag{154}$$

$$E_- = A^-\psi_{00} + B^-\psi_{10} + C^-\psi_{01}, \tag{155}$$

where the A's, B's, and C's are the complex amplitudes of the $\text{TEM}_{00}$, $\text{TEM}_{10}$, and $\text{TEM}_{01}$ fields respectively, and the superscript denotes the frequency (carrier, SB+, or SB-) of the field. Then after a lot of algebraic manipulation, we get,

$$\begin{aligned} A = E_0\overline{E_-} + E_+\overline{E_0} &= g_{00,\overline{00}}|\psi_{00}|^2 + g_{10,\overline{10}}|\psi_{10}|^2 + g_{01,\overline{01}}|\psi_{01}|^2 \\ &\quad + g_{00,\overline{10}}\psi_{00}\overline{\psi_{10}} + g_{00,\overline{01}}\psi_{00}\overline{\psi_{01}} + g_{10,\overline{01}}\psi_{10}\overline{\psi_{01}}, \end{aligned} \tag{156}$$

where

$$g_{00,\overline{00}} = A^c\overline{A^-} + A^+\overline{A^c}, \tag{157}$$

$$g_{10,\overline{10}} = B^c\overline{B^-} + B^+\overline{B^c}, \tag{158}$$

$$g_{01,\overline{01}} = C^c\overline{C^-} + C^+\overline{C^c}, \tag{159}$$

$$g_{00,\overline{10}} = A^c\overline{B^-} + A^-\overline{B^c} + A^+\overline{B^c} + A^c\overline{B^+}, \tag{160}$$

$$g_{00,\overline{01}} = A^c\overline{C^-} + A^-\overline{C^c} + A^+\overline{C^c} + A^c\overline{C^+}, \tag{161}$$

$$g_{10,\overline{01}} = B^c\overline{C^-} + B^-\overline{C^c} + B^+\overline{C^c} + B^c\overline{C^+}. \tag{162}$$

Now one can use (148) to calculate the demodulated signal.

### 4.4.5 Quad Photodiodes

Since the $\text{TEM}_{mn}$ modes are orthogonal over all space, then if S is measured on a regular photodiode, all the cross terms between different modes cancel in the above calculations.

| In Quadrant | $|\psi_{00}|^2$ | $|\psi_{10}|^2$ | $|\psi_{01}|^2$ | Integral of $\psi_{00}\overline{\psi_{10}}$ | $\psi_{00}\overline{\psi_{01}}$ | $\psi_{10}\overline{\psi_{01}}$ |
|---|---|---|---|---|---|---|
| 1 | $1/4$ | $1/4$ | $1/4$ | $1/\sqrt{8\pi}$ | $1/\sqrt{8\pi}$ | $1/2\pi$ |
| 2 | $1/4$ | $1/4$ | $1/4$ | $-1/\sqrt{8\pi}$ | $1/\sqrt{8\pi}$ | $-1/2\pi$ |
| 3 | $1/4$ | $1/4$ | $1/4$ | $-1/\sqrt{8\pi}$ | $-1/\sqrt{8\pi}$ | $1/2\pi$ |
| 4 | $1/4$ | $1/4$ | $1/4$ | $1/\sqrt{8\pi}$ | $-1/\sqrt{8\pi}$ | $-1/2\pi$ |

Table 1: This table gives the integrals of the products of different $\text{TEM}_{mn}$ modes in the four quadrants. These values are critical to calculating pitch and yaw signals.

If, however, we have the fields centered on a photodiode with four separate quadrants, then the cross terms do not cancel. Table 1 gives the integrals of the products of $\text{TEM}_{mn}$ modes; each is given over the four quadrants transverse to the propagation direction.

To calculate pitch and yaw signals, one needs to calculate the demodulated field in each quadrant:

$$S_i = \int\int_{Q_i} (Ae^{-i\phi} + \overline{A}e^{i\phi})\, \mathrm{d}x\, \mathrm{d}y \,. \tag{163}$$

This integration will require many applications of the table above.

To calculate pitch and yaw signals, one needs to take various linear combinations of the $S_i$'s:

$$Pitch = S_1 + S_2 - S_3 - S_4 \tag{164}$$
$$Yaw = S_1 - S_2 - S_3 + S_4 \,. \tag{165}$$

# 5  Wave Front Sensing Time-Domain Modelling

In this section, the details of the Simulink model will be explained in full.

Simulink is a Matlab program that solves differential equations in discrete or continuous time. The model is constructed as a block diagram, and Simulink steps through each point in time, making all necessary calculations before proceeding to the next value of time.

In this model, the positions of the MC and PZT mirrors and the laser coming from the pre-stabilized laser (PSL), along with a myriad of parameters[27] are used to determine the intensity falling on the WFS photodiodes at any given time. These fields then determine an error signal that is fed back to the mirrors to correct their position. Transfer functions for the mirrors can be added to simulate the dynamic response of the system, noise can be added at any point in the loop, and filters can be designed and optimized for noise suppression.

The model uses the formalism described in this paper to calculate the perturbations of the electric fields caused by the time-varying misalignments of the mirrors (PZT and MC).

---

[27]These parameters will be discussed in Section 5.1.

## 5.1 Model-Wide Parameters

Simulink has the property that signals can be sent to various parts of the model remotely. The pentagonal blocks are remote sending and receiving blocks. These allow for all the model-wide parameters to be input on the front end of the model, rather than having to input them multiple times. Additionally, the remote property allows for a cleaner appearance, because multiple wires do not need to be drawn from the parameters to their corresponding blocks.
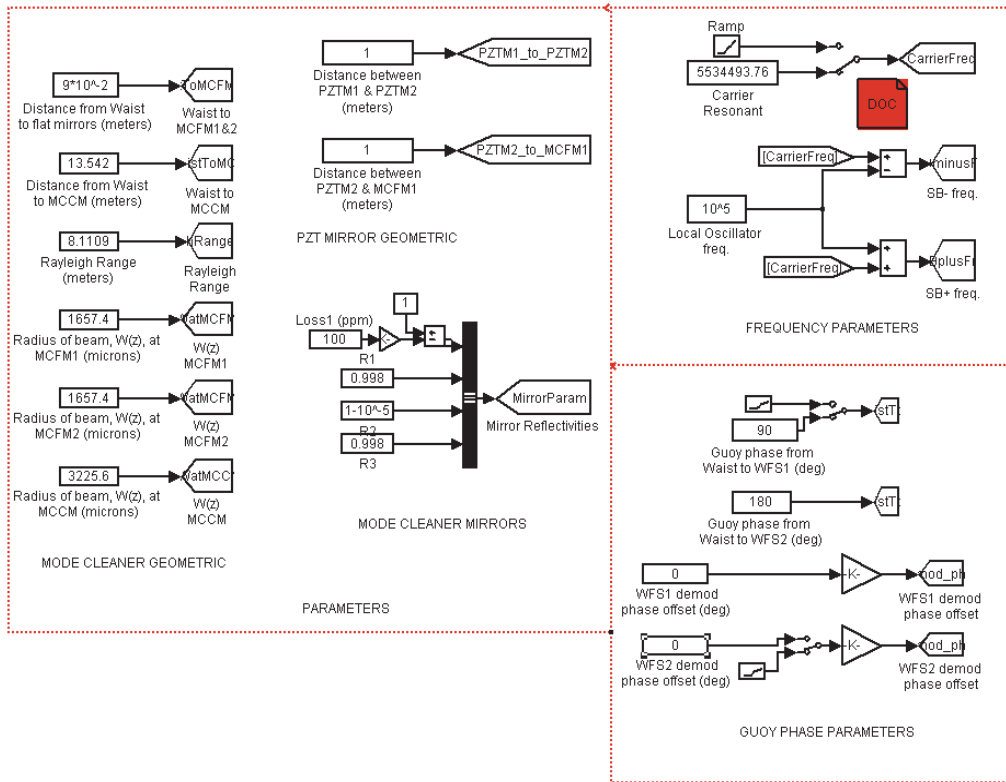


Figure 21: All global parameters are entered on a single screen; they are broadcast to all relevant subsystems by the pentagonal blocks.

The model has a multitude of parameters which need to be set/understood.

Figure 21 shows all the parameters which can be set within the model, with the exception of the field amplitudes themselves.

### 5.1.1 Mode Cleaner Geometric and Reflectivities

Referring back to Figure 21, first, the geometric properties of the mode cleaner must be set. These are the parameters in the box labeled "PARAMETERS."

Eventually, the geometric parameters will be reduced to just three geometric parameters: the distance from Waist to flat mirrors, the distance from waist to curved mirror, and the radius of curvature of the curved mirror. The rest of the parameters can be calculated using these three numbers.

Presently, the numbers must be calculated "by hand." This can be done quite easily with the resonator algebra defined in Section 4.1.5 and the definitions of the auxiliary functions in section 4.1.1.

Next the PZT mirror geometry must be set. This is simply the distance between the two PZT mirrors.

The next set of parameters is the set of mirror reflectivities and losses. These are the *Power* reflectivities and losses. Currently, the total round trip loss (the combined loss is lumped into the loss of the first mirror) is 100 parts per million (ppm).

### 5.1.2 Frequency Parameters

The next group of parameters are the "FREQUENCY PARAMETERS" in Figure 21.

The free spectral range (FSR) of the cavity is 11.0689 MHz. The carrier must be an odd multiple of half the free spectral range to be resonant in the mode cleaner. This resonance condition is derived using the sign convention that light aquires a pi phase shift when reflecting off the coated side of an optic.

For the model to work properly, the carrier must be resonant in the mode cleaner. The first frequency at which the carrier is resonant is 5534463.76 Hz. The fact that the actual laser frequency is millions of FSRs does not matter for the model. Additionally, the carrier frequency can be ramped for diagnostic purposes; to ramp the frequency, connect the switch to "Ramp" instead of "Carrier Resonant."

The local oscillator frequency must also be set. This is the frequency at which the electro-optic modulators are driven; thus, this is the modulation frequency of the sidebands. Currently at the 40m, the MC sideband frequency is 29.486 MHz.

### 5.1.3 Guoy Phase Parameters

The next set of parameters refer to those marked "GUOY PHASE PARAMETERS" in Figure 21.

Unlike the real system, the model easily facilitates changing the Guoy phase telescopes. Currently, the two wavefront sensors are set at 90 degrees and 180 degrees [9]. Using the model, it is simple to explore the effects of changing the WFS positions in Guoy phase.

Additionally, the model allows one to look at an arbitrary demodulation phase. Thus, one can quickly switch back and forth between I (0 degrees) and Q (90 degrees). Currently, both WFS are looking at I phase [9].

### 5.1.4 Field Amplitudes and Phases

Figure 22 shows the blocks that multiply the input coupling matrix to find the amplitudes and phases of the carrier and sidebands.

The amplitudes of the fields must be input. For things to make sense, the absolute values of the amplitudes should add to unity; this is currently satisfied as $|0.90| + |-0.05| + |0.05| = 1$. In addition, it is *imperative* that the sign of the SB- field be negative. This is because the definition of phase modulation sidebands puts the two sidebands $\pi$ out of phase with one another.

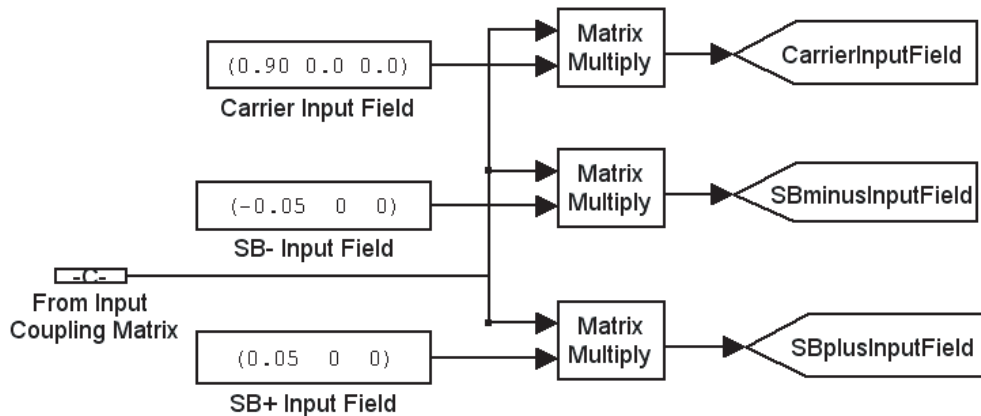These fields are sent remotely to many blocks within the model.

Figure 22: The amplitudes of the fields are entered into these blocks; the sum of the amplitudes should be one.
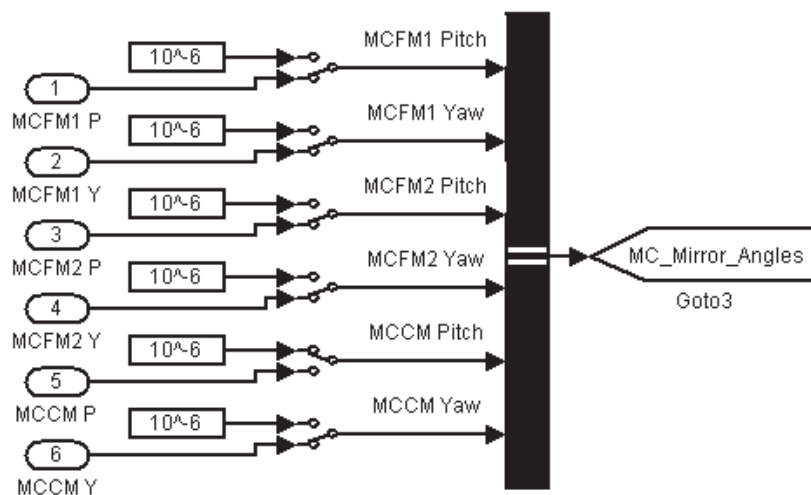


Figure 23: The dynamic pitch and yaw angles of the MC mirrors are controlled by these blocks. They can be easily switched from closed-loop positions to open-loop constant offsets, which are useful for diagnostics.

## 5.2   Dynamic Alignment of Mirrors and PSL

### 5.2.1   Mode Cleaner Mirrors: Pitch and Yaw

The group of blocks that determines the alignment of the MC mirrors is shown in Figure 23. The pitch and yaw angles of the mirrors are input in radians. All six angular degrees of freedom are independent.

The switches should be kept on the round inputs, which completes the feedback loop. However, for diagnostic purposes, constant offsets have been set to one microradian. In addition to these constant offsets, a sinusoidal input or ramp may replace any of the static misalignments.

The six mirror angles are combined into a single signal via the "bus" block, which is the long black

bar. This single signal is then broadcast to the rest of the model.
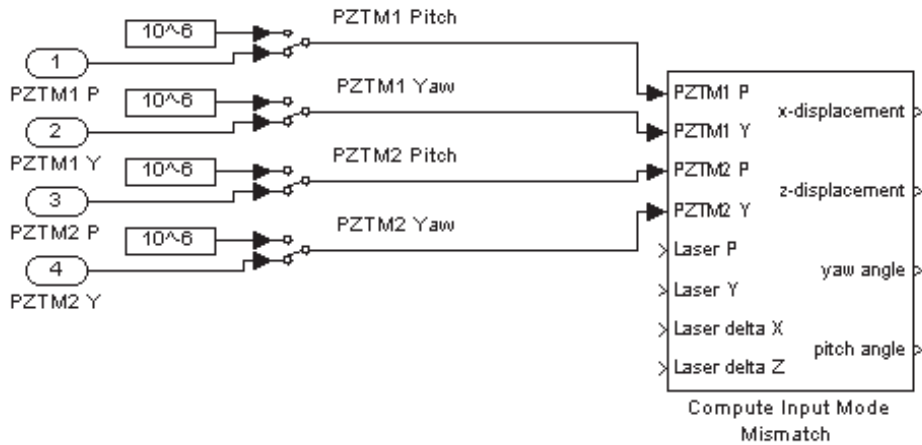
### 5.2.2 PZT Mirrors: Pitch and Yaw



Figure 24: The dynamic pitch and yaw angles of the PZT mirrors are controlled by these blocks. The open input ports receive information about the PSL.

The group of blocks that determines the alignment of the PZT mirrors is shown in Figure 24. Just like the MC mirrors, the pitch and yaw angles of the mirrors are input in radians. All four angular degrees of freedom are independent.

Again, for closed loop operation, the switches should be set to the round input blocks. The constant offsets are only there as diagnostic tools.

### 5.2.3 PSL: Angles and Offsets

At PZT mirror 1, the PSL beam will be travelling at an angle to its ideal path; it will also be offset from this path. These deviations adversely affect the coupling to the mode cleaner and are essentially noise.

Figure 25 shows the blocks which govern these deviations of the PSL input laser beam. Like the other dynamic parameters, in normal operation the switches will be set to the round input blocks, and diagnostics can be done with the constant deviations.

## 5.3 Mode Cleaner Reflectivity Matrices

From (125), we see that the reflectivity matrix is a complicated function of matrices, involving products, sums, and inverses. A central role is played by $\mathbf{G}_{rt}$, the round trip operator, which is itself the product of 6 matrices. Of the 6 matrices involved in the reflectivity matrix, the three mirror alignment matrices are dynamic and the three propagators are static.

Figure 26 shows the block that broadcasts the reflectivity matrix to the rest of the model. For each of the three fields (carrier and two sidebands), 21 subsystems in four sub-levels are contained within this block. Fortunately, the 21 subsystems are *almost* identical for all three fields, which makes constructing
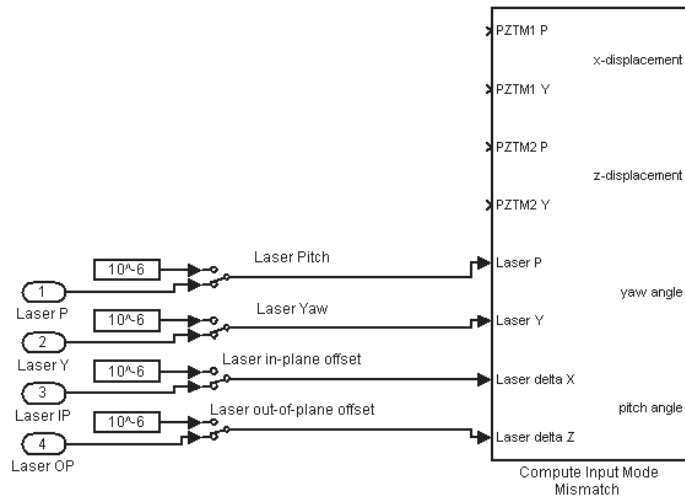
Figure 25: The dynamic PSL inputs consist of the pitch and yaw angles (radians) and the offsets (meters) in and perpendicular to the plane of the interferometer. These inputs are measured at PZT mirror 1. The open input ports receive information about the PZT mirrors.

three no harder than one. They differ, of course, in the propagator matrices because the sidebands are at different frequencies than the carrier. This change is easily made using the broadcast sideband frequencies shown in Figure 21.

### 5.3.1 Round Trip Operator

The bulk of the work that goes into computing the reflectivity matrix goes into calculating the round trip operator (RTO). Figure 27 shows the RTO subsystem.

Three misalignment matrices, three free space propagation matrices[28], and the flip operator[29] are multiplied in the center of the system to yield the round trip operator defined in (127).

### 5.3.2 RTO: Misalignment Matrices

The three matrices on the left are the adjoints of the misalignment operators (82) and (83). However, only the fields incident on the curved mirror are at normal incidence when aligned; thus, the coefficients that multiply the normalized angles in (82) and (83) are not two for the flat mirrors[30].

Inside the "MCCM Misalignment (M3) Matrix (adjoint) Subsystem" block shown in Figure 28, there is a series of subsystems that performs simple operations: the angles are normalized, and the matrix is concatenated from its scalar elements. The blocks that perform these operations are shown in Figure 29.

The system takes as its inputs the dynamic alignment angles of the curved mirror; it also takes the width of the beam at that mirror, $w(z)$ at MCCM, which is broadcast by the "PARAMETERS" box shown in Figure 21.

---

[28]The construction of these matrices is discussed in the following sections
[29]The flip operator is discussed in Section 4.3.2.
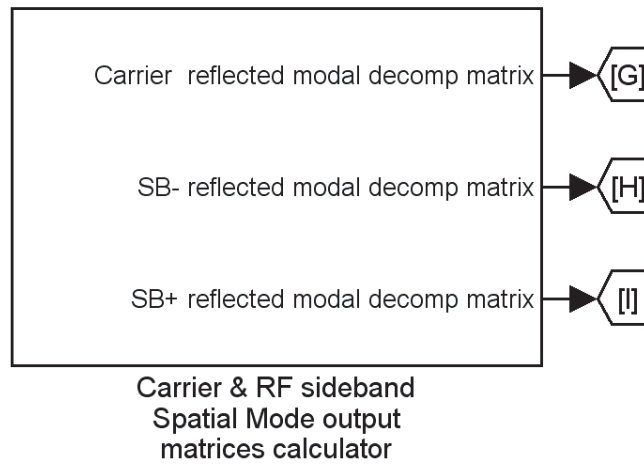[30]Refer to the discussion in Section 4.2.8.

Figure 26: Within this block, the reflectivity matrix of the MC is constructed. Since the mirror alignments are dynamic, so too is the reflectivity matrix.

The angles passed to the reflection matrix must be normalized per the discussion in Section 4.2.5. Figure 30 shows how this is accomplished. The angle is simply multiplied by $\pi w(z)/\lambda$.

After the angles have been normalized, they are passed to the block labelled "MCCM Misalignment Matrix Generator." The contents of this block are shown in Figure 31. The subsystem is responsible for the concatenation of the normalized misalignment angles and various constants into the misalignment matrix.
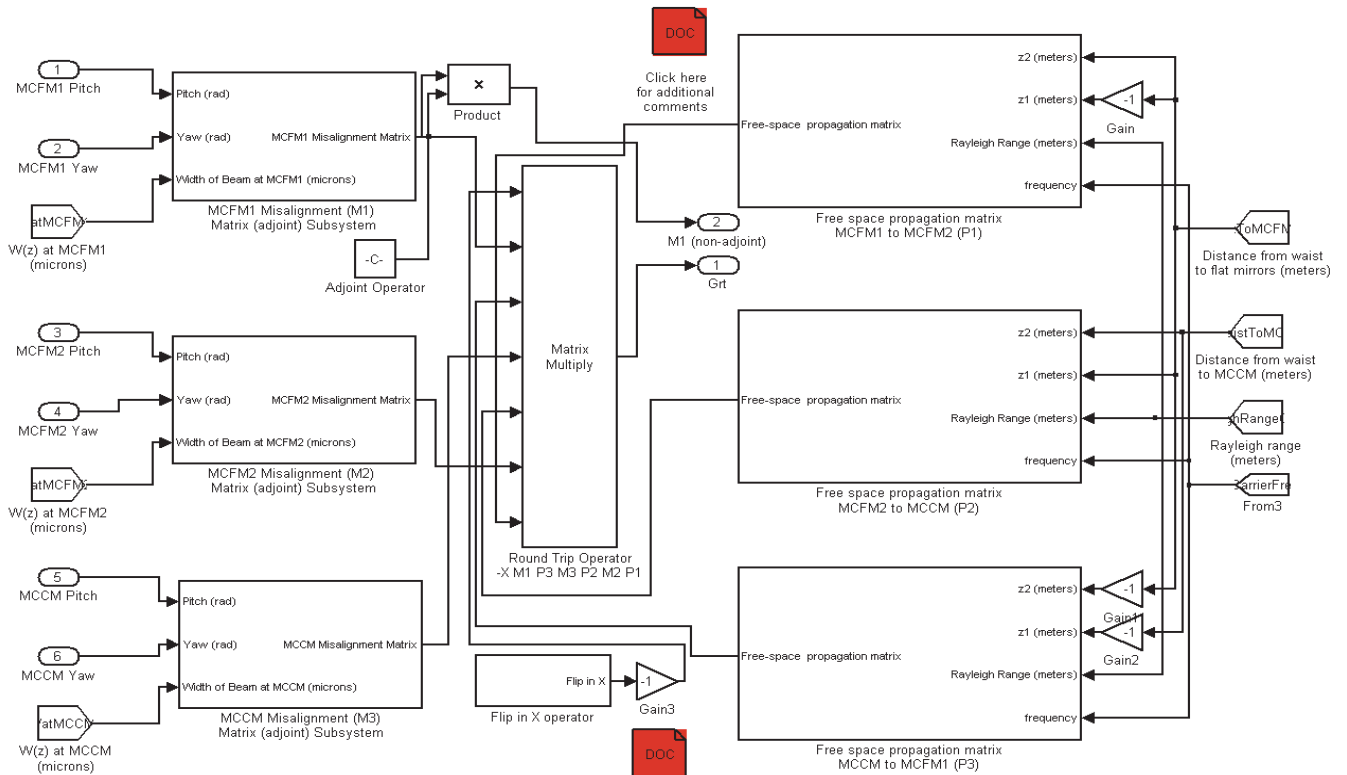
Figure 27: This subsystem calculates the round trip operator (127) based on the dynamic MC mirror angles and the global parameters discussed in Section 5.1.
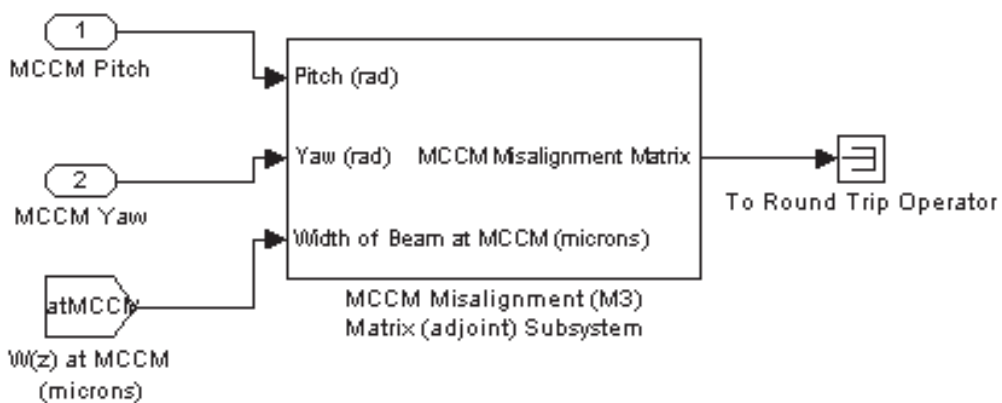


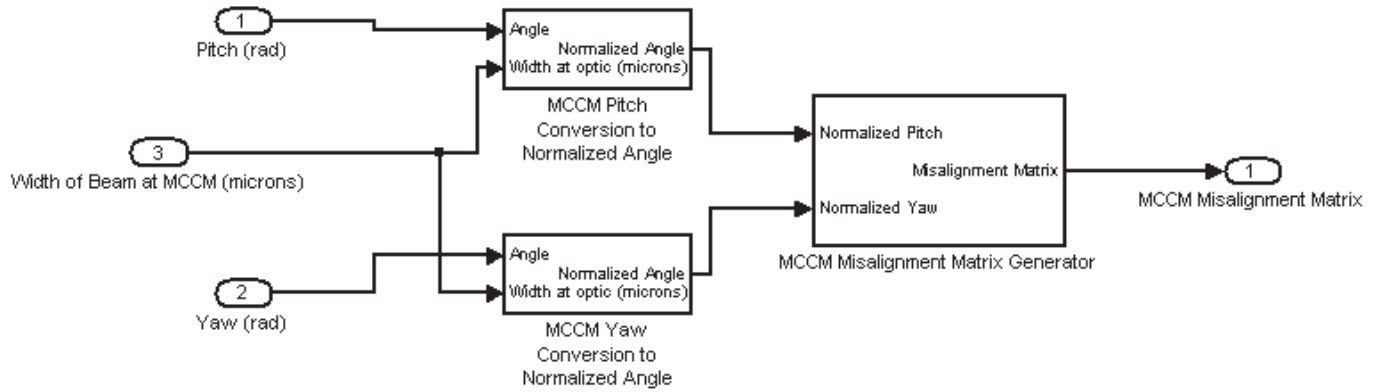Figure 28: This block constructs the reflection matrix for the curved mirror (MCCM).

44

Figure 29: The innards of the MCCM reflection matrix block normalizes the misalignment angles using the width of the beam, and concatenates the normalized angles (after being multiplied by the proper complex constants) into the reflection matrix (adjoint).
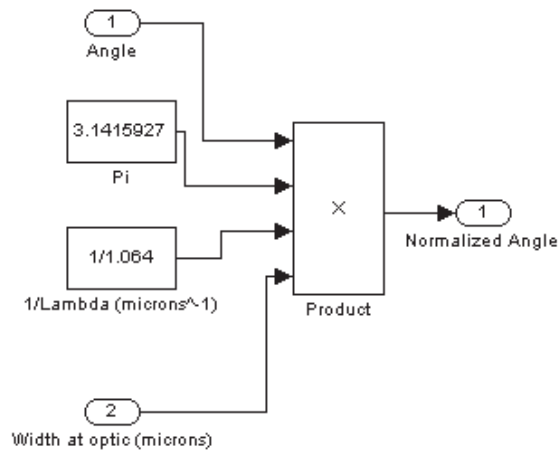


Figure 30: The angle normalization block performs the requisite multiplication.
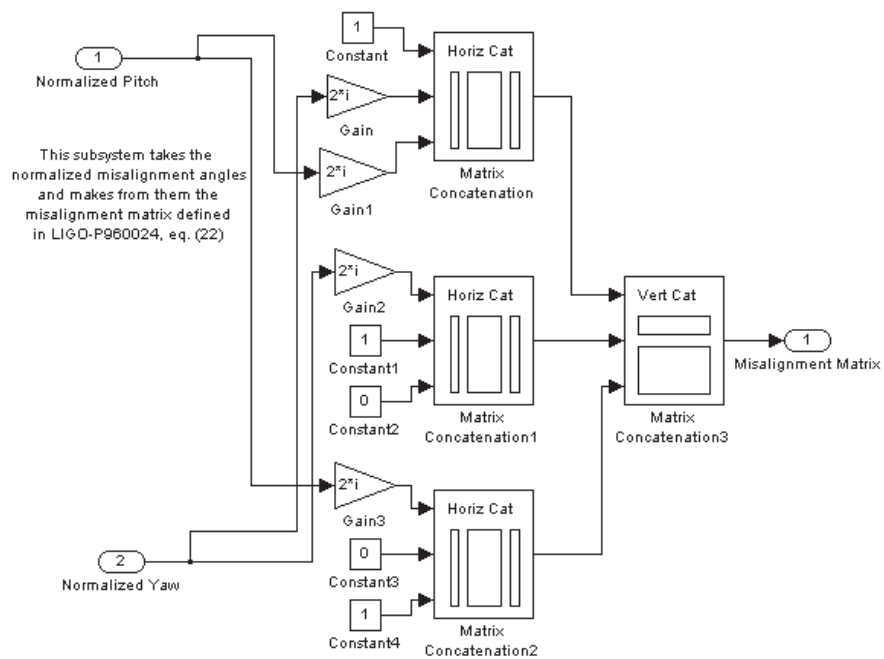
Figure 31: The MCCM misalignment matrix generator concatenates the normalized misalignment angles and various constants into the misalignment matrix.

This completes the description of the misalignment matrix. Each mirror has its own group of subsystems which creates and constantly updates the elements of the matrix. The only difference between the matrices of different mirrors are the numerical coefficients that multiply the normalized misalignment angles and the angles themselves.
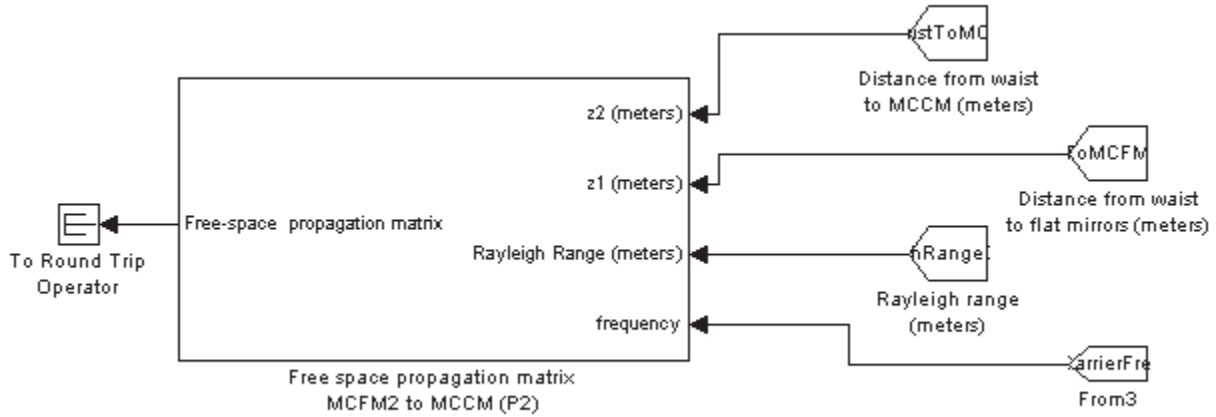
### 5.3.3 RTO: Free Space Propagators



Figure 32: The free space propagator can continually update the accumulated phase, although the only thing that would change dynamically might be the carrier frequency.

The free space propagator is responsible for the accumulated phase (Guoy and bulk length) of a mode as it propagates around the optical cavity. It takes as its inputs the distance from the waist to each of the points to which it will propagate; it also takes the Rayleigh range and frequency of the radiation. These features are shown in Figure 32

Figure 33 shows the contents of the free space propagator. The frequency is multiplied by $-i2\pi/c$ and then the length, and that product is exponentiated to make $e^{-ikl}$.

The distances from the waist to each point and the Rayleigh range are used to construct terms like $Prop(z_1, 0) = \arctan[z_1/z_0]$, which is the Guoy phase accumulated propagating from the waist to $z_1$. The difference $Prop(z_2, 0) - Prop(z_1, 0)$ is one unit of accumulated Guoy phase, and this quantity is concatenated to make the free space propagation matrix defined in (90).

### 5.3.4 Reflectivity Matrix Calculator

Figure 34 shows the remaining subsystems used to calculate the reflectivity matrix. The outputs of the "Round Trip Operator Subsystem" are the round trip operator and the misalignment matrix of MCFM1. These matrices, together with the mirror parameters from Figure 21, are combined in various combinations to make the reflectivity matrix defined by (125).
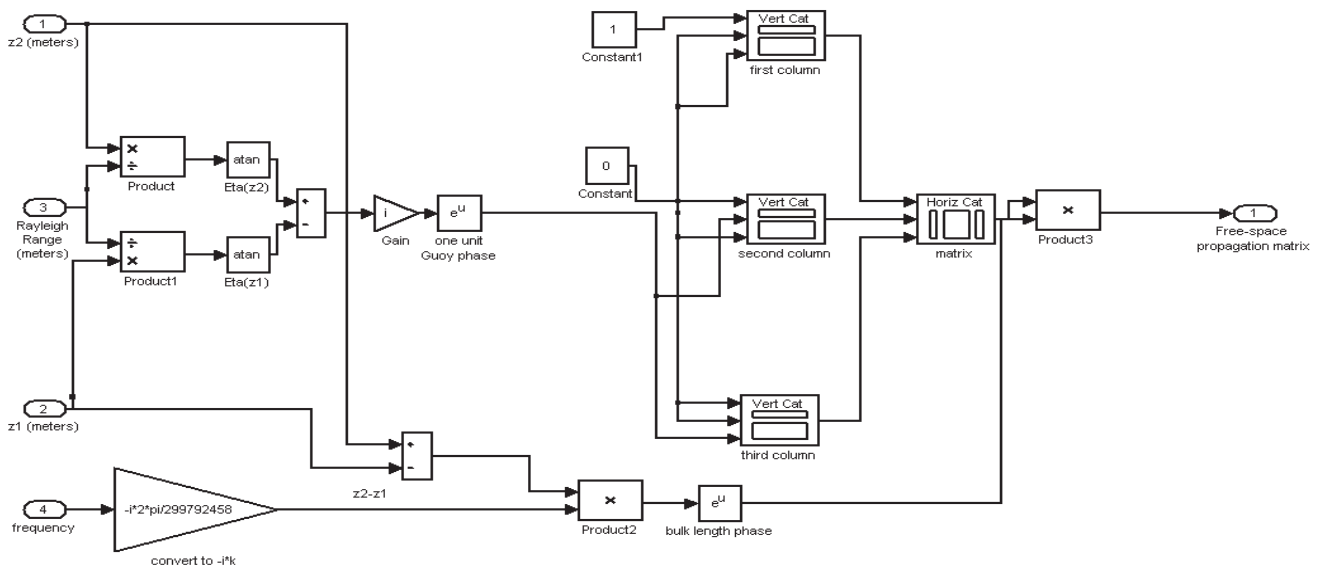
47

Figure 33: The free space propagator contains blocks that compute the bulk length phase and Guoy phase accumulated between two points.
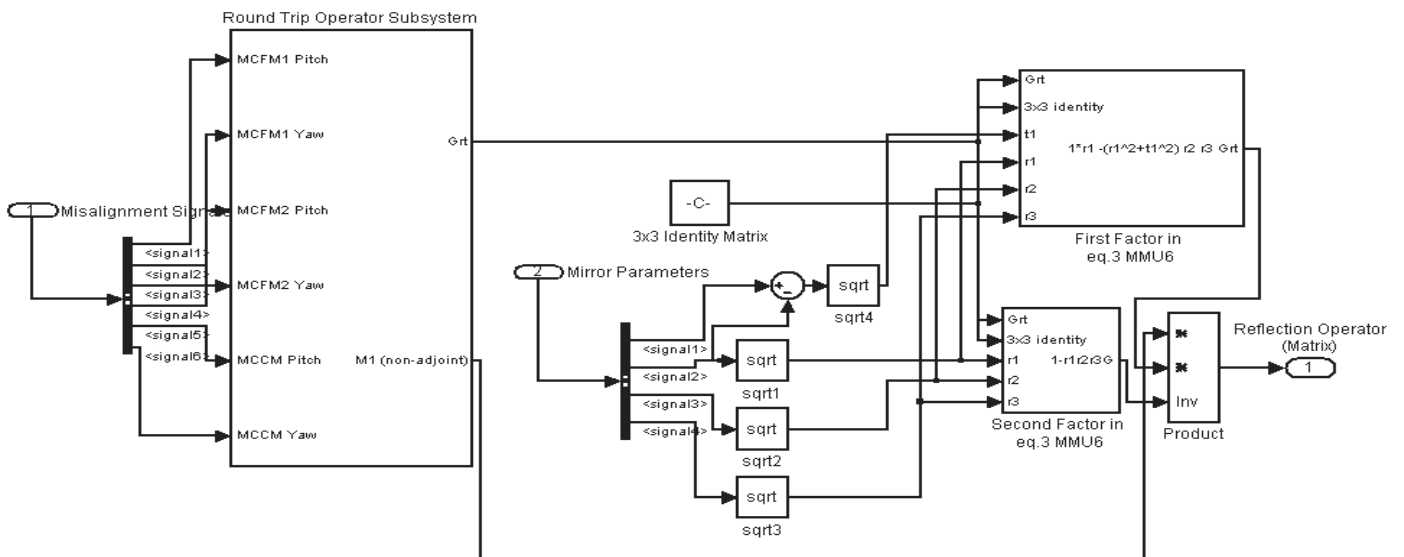


Figure 34: This group of subsystems performs the remaining calculations to make the reflectivity matrix.

### 5.3.5 Reflected Fields

The model generates three reflectivity matrices, one for the carrier, upper sideband, and lower sideband. These matrices are identical except for the frequency of the field they deal with.

The next step is to multiply each of the three input fields by the corresponding reflectivity matrix. This then gives the amplitude and phase of the $TEM_{00}$, $TEM_{10}$, and $TEM_{01}$ fields for each of the three frequencies. This makes a total of 9 fields.
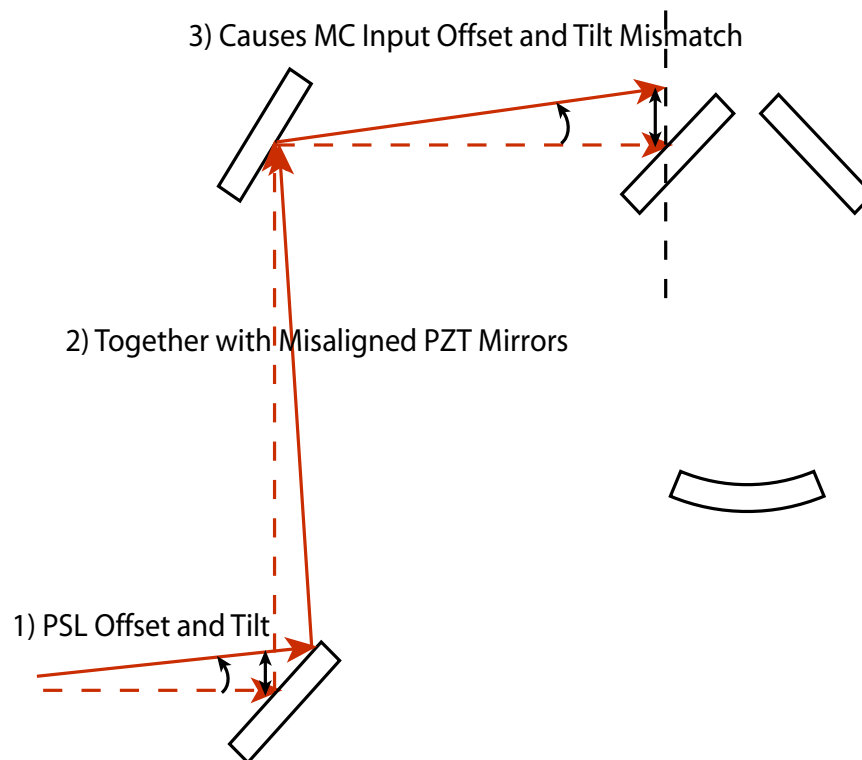
## 5.4 Input Coupling



Figure 35: This illustration shows how the input mode can be mismatched to the requisite cavity mode.

Figure 35 shows the basic problem with input coupling. The cavity has a well-defined axis along which its eigenmodes must propagate. If the input laser beam is offset or tilted from this ideal direction, then it will not couple efficiently to the mode cleaner (MC). One problem with this is that not as much light will be coupled through the MC, which decreases potential gravitational wave signals. In addition, the light that does not couple to the MC will be reflected, which will distort the error signal used to control the alignment of the MC. One must then decide whether it is better to move the MC mirrors to match the input mode or move the PZT mirrors to match the input mode to the MC; if one does not decide in advance, then the meaning of the ASC error signal will be ambiguous.

There are 8 degrees of freedom which must be controlled to steer the laser into the MC: PSL offset in and out of the plane of the MC (2), PSL pitch and yaw tilts (2), PZTM1 pitch and yaw (2), and PZTM2 pitch and yaw (2). The program has no problem keeping track of all these degrees of freedom,

49

but calculating what the tilts and offset at the MC will be in terms of these 8 degrees of freedom is non-trivial. The next few sections deal with how these calculations are done.

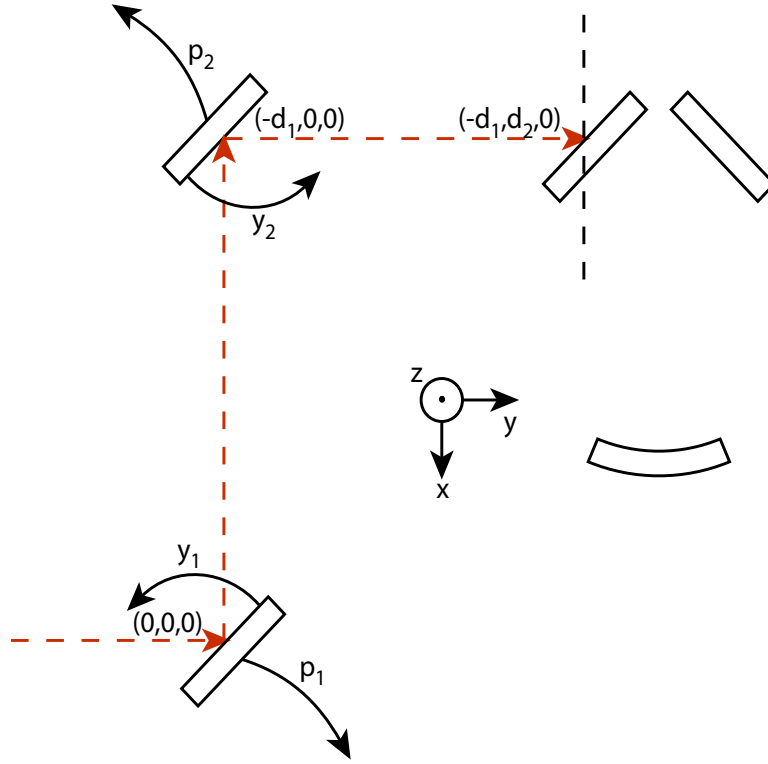### 5.4.1 Analytical Calculations of Input Coupling



Figure 36: The geometric definitions of the PSL path include directions of positive increase for all PZT mirror angles and the distances between the pivot points (centers) of the PZT mirrors.

Figure 36 shows the geometry of the laser input path. The PSL inputs a beam that has an offset in both the $z$ and $x$ directions; these will be called $\Delta x_L$ and $\Delta z_L$. It also has an initial tilt in the $x - y$ ($y_L$) and $y - z$ ($p_L$) planes. The two PZT mirrors have their pitch and yaw angles defined according to Figure 36.

To calculate the final misalignments of the beam when it reaches the first mode cleaner mirror, we will need to calculate how the original misalignments of the PSL propagate through arbitrarily misaligned PZT mirrors to become the final misalignments.

Consider the case of a line passing through the point $p_{line} = (x_{line}, y_{line}, z_{line})$, whose direction is given by a vector $\vec{\mathbf{k}} = \langle k_x, k_y, k_z \rangle$[31]. Also consider a plane containing the point $p_{plane} = (x_{plane}, y_{plane}, z_{plane})$ and having a unit normal vector $\hat{\mathbf{n}} = \langle n_x, n_y, n_z \rangle$. Figure 37 illustrates this situation.

The parameterized equation of the line can be obtained with elementary vector analysis:

$$x = tk_x + x_{point} \quad y = tk_y + y_{point} \quad z = tk_z + z_{point}, \tag{166}$$

---

[31]I have chosen to use **k** because it will turn out that it doesn't matter if the vector is normalized, and the k-vector of a ray is in the direction of propagation.
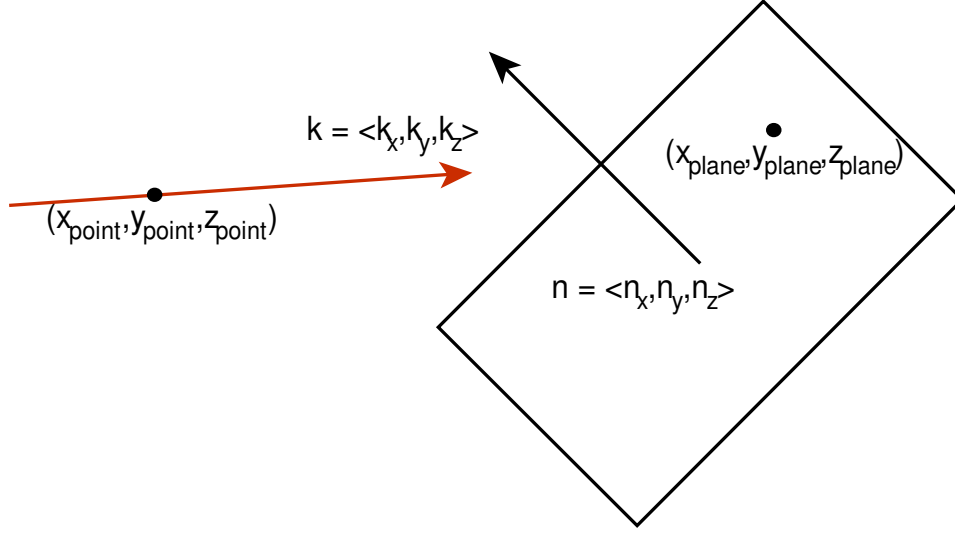
Figure 37: A line passing through the point $p_{line} = (x_{line}, y_{line}, z_{line})$ with vector $\mathbf{k} = \langle k_x, k_y, k_z \rangle$ travels towards a plane with unit normal $\hat{\mathbf{n}} = \langle n_x, n_y, n_z \rangle$ and point $p_{plane} = (x_{plane}, y_{plane}, z_{plane})$.

where t is an arbitrary constant that parameterizes the line.

The equation of the plane is

$$(x - x_{plane})n_x + (y - y_{plane})n_y + (z - z_{plane})n_z = 0 \,. \tag{167}$$

If the vector is not parallel to the plane, then substituting the values of x, y, and z from 166 into 167 yields a single equation that can be solved for t:

$$t = -\frac{\vec{\boldsymbol{\Delta}} \cdot \hat{\mathbf{n}}}{\vec{\mathbf{k}} \cdot \hat{\mathbf{n}}} \,, \tag{168}$$

where

$$\vec{\boldsymbol{\Delta}} \equiv \langle x_{point} - x_{plane}, y_{point} - y_{plane}, z_{point} - z_{plane} \rangle \,. \tag{169}$$

Substituting this value for t back into 166 gives the point at which the line and plane intersect:

$$x_{intersection} = x_{point} - \frac{\vec{\boldsymbol{\Delta}} \cdot \hat{\mathbf{n}}}{\vec{\mathbf{k}} \cdot \hat{\mathbf{n}}} k_x \,, \tag{170}$$

$$y_{intersection} = y_{point} - \frac{\vec{\boldsymbol{\Delta}} \cdot \hat{\mathbf{n}}}{\vec{\mathbf{k}} \cdot \hat{\mathbf{n}}} k_y \,, \tag{171}$$

$$z_{intersection} = z_{point} - \frac{\vec{\boldsymbol{\Delta}} \cdot \hat{\mathbf{n}}}{\vec{\mathbf{k}} \cdot \hat{\mathbf{n}}} k_z \,. \tag{172}$$

Now, suppose the plane were a mirror, the ray would reflect with a new k-vector, $\vec{\mathbf{k}}'$, given by the vector law of reflection (84). The reflected ray defines a new line with $\vec{\mathbf{k}}'$, and it would definitely pass through the point $(x_{intersection}, y_{intersection}, z_{intersection})$, since the ray is continuous. In addition, it is natural to use the center of the PZT mirror for the point contained by the plane; the mirror pivots around this point, which means it is the *only* point that is always on the plane.

This then allows us to determine what the final misalignment of the PSL beam is after it propagates to the first MC mirror. Refer to Figure 36 as the following procedure is explained.

1) The incoming beam is a line that passes through the point $p_0 = (\Delta x_L, 0, \Delta z_L)$ and $\vec{k_0} = \langle -\sin(y_L), \cos(y_L)\cos(p_L), \cos(y_L)\sin(p_L) \rangle \approx \langle -y_L, 1, p_L \rangle$.

2) The first PZT mirror has unit normal $\hat{n}_1 \approx \langle \frac{1}{\sqrt{2}} y_1 - \frac{1}{\sqrt{2}}, -\frac{1}{\sqrt{2}} y_1 - \frac{1}{\sqrt{2}}, p_1 \rangle$ and pivots around the point $(0, 0, 0)$.

3) Use (84) to calculate the reflected k-vector, $\vec{k}'$, using the incident k-vector and the first PZT normal.

4) Calculate the point of intersection, $p_{int,1}$, for the first line and PZT mirror.

5) The reflected beam is now a line passing through $p_{int,1}$ with $\vec{k}'$.

6) The second PZT mirror has unit normal $\hat{n}_1 \approx \langle \frac{1}{-\sqrt{2}} y_2 + \frac{1}{\sqrt{2}}, \frac{1}{\sqrt{2}} y_2 + \frac{1}{\sqrt{2}}, p_2 \rangle$ and pivots around the point $(-d_1, 0, 0)$.

7) Use (84) to calculate the reflected k-vector, $\vec{k}''$, using $\vec{k}'$ and the second PZT normal.

8) Calculate the point of intersection, $p_{int,2}$, for the second line and PZT mirror.

9) The reflected beam is now a line passing through $p_{int,2}$ with $\vec{k}''$.

10) The last normal vector is $\langle 0, 1, 0 \rangle$, which is normal to the plane passing through the center of the first MC mirror at $(-d_1, d_2, 0)$. This is the plane at which the misalignments will be defined and the coupling to the mode cleaner calculated.

11) The last intersection is calculated using the second reflected line and the above-mentioned plane. Call this intersection $(x_{int,3}, d_2, z_{int,3})$.

12) The final offset in x is $\Delta x = x_{int,3} + d_1$.

13) The final offset in z is $\Delta z = z_{int,3}$.

14) The final yaw tilt is $yaw = -\arctan(k_x''/k_y'')$.

15) The final pitch tilt is $pitch = \arctan(k_z''/k_y'')$.

All of the normals to the mirrors in the above procedure were calculated using (88).

### 5.4.2 Model Calculations of Input Coupling

The input coupling is calculated by the model according to the method described in Section 5.4.1. Figure 38 shows the block that does the bulk of the work. It takes as its inputs the initial k-vector of a beam, a point through which the line passes, the mirror's unit normal, and the mirror's pivot point[32]. Its output is the new line's normal vector and the point at which the incoming beam and mirror intersect. These outputs can then be fed to another identical block, and so the final misalignment can be found iteratively.

For the sake of brevity, the innards of the block will not be shown here, but they simply do exactly the same steps as were described in Section 5.4.1.

---

[32]To facilitate calculations, all points $(x, y, z)$ should be fed to the block as a vector $\langle x, y, z \rangle$.
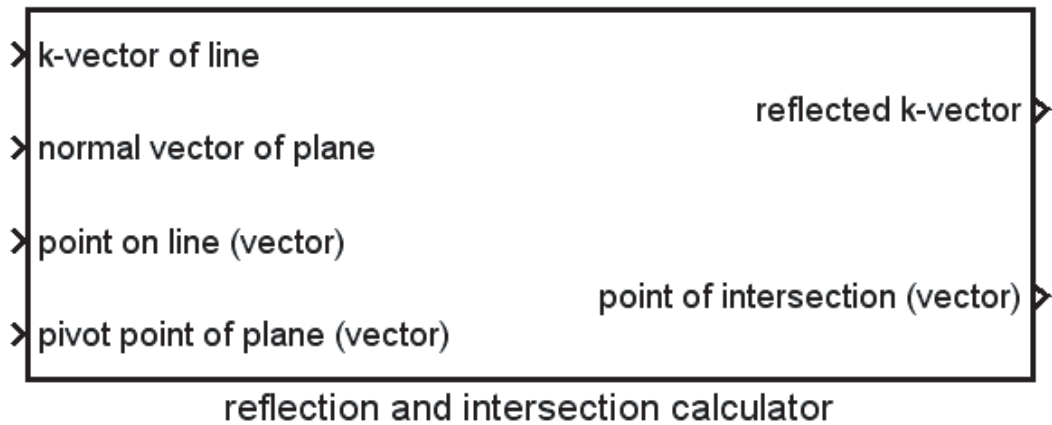
Figure 38: This block calculates the line of the reflected beam based on the incoming beam's direction and fixed-point and mirror's unit normal and pivot point.

### 5.4.3 Coupled Fields

The subsystems described in Section 5.4.2 continuously update the input coupling into the mode cleaner. With that information, the tilt and offset matrices are calculated according to Sections 4.2.5 and 4.2.4 respectively.

These matrices multiply the input fields shown in Figure 22. The resulting vectors are the fields that will couple to the Mode Cleaner; thus, it is these fields that will be multiplied by the reflectivity matrices.

## 5.5 WFS Signals

### 5.5.1 Guoy Phase Telescopes

After the input-coupled fields are multiplied by the reflectivity matrices, the reflected fields are sent to another free space propagation matrix. This propagation matrix represents the Guoy phase telescope, and allows one to tune the relative phases of the different $\text{TEM}_{mn}$ modes.

Actually, two identical copies are made of the reflected fields, and each one is sent to a different Guoy phase telescope.

### 5.5.2 QPD

After the Guoy phase telescopes, the fields fall on the quad photodiodes (QPD). At this point, each of the nine field components (3 frequencies x 3 spatial modes) are separated into separate components. From these separate components, the calculations follow the work in Sections 4.4.3 through 4.4.5.

### 5.5.3 ASC Error Signals

After the fields from various quadrants are combined to make the pitch and yaw error signals, the optical plant is complete.

## 5.6 Results

The current state of the model is such that only a limited number of things can be tested.

### 5.6.1 PZT Control Matrix

One significant thing that has been done is the development of a PZT mirror control matrix. By moving the PZT mirrors in such a way that only pitch, yaw, or either offset is produced at the first MC mirror, one can deduce a numerical control matrix for the values of the parameters being tested. By varying the parameters, one can try to deduce the control matrix for arbitrary parameters.

If the PZT mirrors are tilted such that

$$p_1 = \text{arbitrary} \tag{173}$$
$$y_1 = 0 \tag{174}$$
$$p_2 = -\frac{d_1 + d_2}{d_2}p_1 \tag{175}$$
$$y_2 = 0 \,, \tag{176}$$

then there will be a tilt in pitch at the first MC mirror without any offset.

If the PZT mirrors are tilted such that

$$p_1 = 0 \tag{177}$$
$$y_1 = \text{arbitrary} \tag{178}$$
$$p_2 = 0 \tag{179}$$
$$y_2 = +\frac{d_1 + d_2}{d_2}y_1 \,, \tag{180}$$

then there will be a tilt in yaw at the first MC mirror without any offset.

If the PZT mirrors are tilted such that

$$p_1 = -p_2 \tag{181}$$
$$y_1 = y_2 = 0 \,, \tag{182}$$

then there will be a tilt a $\Delta z$ offset and no tilt.

If the PZT mirrors are tilted such that

$$p_1 = p_2 = 0 \tag{183}$$
$$y_1 = y_2 \,, \tag{184}$$

then there will be a $\Delta x$ offset and no tilt.

### 5.6.2 A Working Model

The success of the model itself is significant. There are thousands of blocks in hundreds of subsystems, and getting them to work was a challenge.

I have devised several ways of checking the model thus far. First, I built a Mathematica model of a plain Fabry-Perot cavity using methods identical to those explained in this paper. The Fabry-Perot has

trivial behavior, and I was able to derive analytical expressions for many things; the result was that I trusted my methods. Second, I built a Mathematica model of my model; this allowed me to compare the numerical results, and after some debugging, I found the two were identical. Therefore, I have good reason to trust the results of my model.

In addition, I have set up various checks within the Simulink model; one of these checks is to generate the Pound-Drever-Hall error signals for the aligned cavity. The model passes this test with flying colors.

## 5.7 Future Work

### 5.7.1 Mechanical Response

The transfer functions for all mirrors are currently unity. This is okay for the PZT mirrors, whose resonances are well into the hundreds of Hertz, but transfer functions of the MC mirrors are critically important if the model is to be realistic.

### 5.7.2 Noise

Although there are many places at which one could add noise, there is currently no noise being added at any point.

The most important, of course, is the PSL pointing noise. Next in line must be the seismic noise's coupling to the MC mirrors.

### 5.7.3 Filtering

Once frequency dependent noise is added, it will be natural to investigate what the optimal filtering will be for the servo.

### 5.7.4 Optimization of the Real Mode Cleaner

This is, of course, the most important thing of all. Eventually, I hope to use this model to determine the best choice of filters and parameters for the 40m mode cleaner.

Alexei Ourjoumtsev recently did an excellent job bringing the mode cleaner ASC servo online, but it needs to be optimized [9].

# References

[1]  M. Born and E. Wolf. *Principles of Optics*. Cambridge University Press, 1999.

[2]  G. Arfken and H. Weber. *Mathematical Methods for Physicists*. Academic Press, 1995.

[3]  A. Yariv. *Introduction to Optical Electronics*. Holt, Rinehart and Winston, 1976.

[4]  N. Mavalvala. *Alignment Issues in Laser Interferometric Gravitational-Wave Detectors*. PhD thesis, Massachusetts Institute of Technology, 1990.

[5]  D.Z. Anderson. Alignment of resonant optical cavities. *Applied Optics*, 23, 1984.

[6]  B. Bhawal, M. Evans, M. Rakhmanov, and H. Yamamoto. Time domain modal model in End-to-End simulation package. Internal Document LIGO-T990081-02-E, LIGO, 2003.

[7]  E. Hecht. *Optics*. Pearson Addison Wesley, fourth edition, 2001.

[8]  D. Sigg. Modal model update 6: Mode cleaner. Internal Document LIGO-T960118-00-D, LIGO, 1996.

[9]  A. Ourjoumtsev. Development of the 40 meter prototype for advanced ligo. Internal Document LIGO-T030198-00-D, LIGO, 2003.

# 7 Appendix 1: Mode-Matching Program

During the modification of the PSL, Conor Mow-Lowry and I found it necessary to quickly calculate both the focal length and position of two lenses such that a beam waist occurred at a specific location, with a specific size.

Using the work derived in Section 4.1.3, I wrote a program in Mathematica which takes as input two available focal lengths, reasonable guesses for the positions of the lenses, and the desired waist size and position; with these inputs, the program finds an exact solution with real waists.

The program uses Mathematica's algebraic language to find an equation for the position and size of the new waist of a beam with a lens (or mirror) inserted into its path at an arbitrary position; to do this, it uses (27) and (28) from page 12. It then finds the equation of another new waist and position using the beam properties given by the last equation. Then the root-finding program is used to find the solution.

Below is the Mathematica code; it is printed so that it can be typed directly into Mathematica. Additionally, it appears in such a way that it can be copied and pasted directly into Mathematica. If the reader wishes to use the program, I can either send them the Mathematica file or the text file which can be pasted in.

```
\!\(w0toz0[w0_] := \(\(\[Pi]\ w0\^2\)\/\(1064*10\^\(-6\)\)\)\)

(*Converts waist to confocal parameter (mm)*)

w0toz0[0.371]

406.402

\!\(z0tow0[z0_] := \@\(\(1064*10\^\(-6\)\)*z0\)\/\[Pi]\)\)

(*Converts confocal parameter to waist (mm)*)

z0tow0[406.42]

0.371008

\!\(z0prime[f_, z00_, zlens_] :=
    z00\/\(\(\((1 - zlens\/f)\)\)\^2 + \(\((z00\/f)\)\)\^2\)\)

(*finds the new confocal parameter given a lens of focal length f,
    initial confocal parameter z00, and position of lens zlens (all in
    mm)*)

z0prime[343.6,w0toz0[0.371],6*25.4]

237.855

z0tow0[237.855]
```

0.283826

```
\!\(wp[f_, z00_,
      zlens_] := \(zlens + f + \((zlens\/z00)\)\^2*\((zlens - f)\)\)\/\(1 +
\((f\/z00)\)\^2 + \(\((zlens\/z00)\)\^2\) \((1 - \(2
f\)\/zlens)\)\)\)
```

(*finds the new waist position (provided that it is downstream of
    the lens) \ given the same initial parameters as for z0prime*)

wp[343.6,w0toz0[0.371],6*25.4]

384.096

%/25.4

15.1219

(*these numbers match those calculated by Alexi's program*)

z0prime[343.6,237.89,1295.4-384.096]

74.1279

z0tow0[%]

0.158448

wp[343.6,237.89,1295.4-384.096]

1431.8

1431.8037322802506+384.096

1815.9

(*follow these steps to fix a waist's size and position: *)

(*1. find the beam waist position (input) and call this position
    z=0*)

(*2.  find the beam waist size and call this w00*)

(*3.convert w00 to z00 using w0toz0[w00]*)

(*4.  let the position of lens 1 (f=f1) be z1*)

(*5.  let the position of lens 2 (f=f2) be z2*)

(*6. compute z0prime[f1,z00,z1]=z01*)

(*7.  compute wp[f1,z00,z1]=zw1 *) (*note: in both the above
    calculations, z1 is an unspecified parameter*)

(*8.  compute z0prime[f2,z01,z2-zw1]=z02*)

(*9.  the waist size is w02=z0tow0[z02]*)

(*10.  compute wp[f2,z01,z2-zw1]+zw1 = zw2*) (*zw2 is the waist
    position*)

(*11. Use FindRoot to find values of z1 and z2 *) (*such that the
    expressions for zw2 and   w02 are the ones desired*)

(*When all this is done, the program becomes:*)

```
findvalues[f1_,f2_,w00_,w02_,zw2_,guessz1_,guessz2_]:=
  Module[{},z01=z0prime[f1,w0toz0[w00],z1];zw1=wp[f1,w0toz0[w00],z1];
    FindRoot[{z0tow0[z0prime[f2,z01,z2-zw1]]\[Equal]w02,
        wp[f2,z01,z2-zw1]+zw1\[Equal]zw2},{z1,guessz1},{z2,guessz2}]]
```

(*where
    f1 and f2 are the focal lengths of lens 1 and 2 respectively
    w00 is the input beam's waist radius
    w02 is the desired output beam's waist radius
    zw2 is the desired position of the output beam's waist
    guessz1 and guessz2 are initial guesses for the positions of lens 1 and
    respectively*)

(*don't forget that if you are not working from z=
    0 you need to shift your coordinates so
    that the input beam's waist is at z=0*)


(*Various solutions are possible depending on the initial guesses
    for z1 and \ z2, as can be seen by the next three outputs:*)

findvalues[343.6,343.6,0.371,0.150,1701.8,152.4,1295.4]

{z1\[Rule]61.6195,z2\[Rule]1169.56}

findvalues[343.6,343.6,0.371,0.150,1701.8,500,1000]

{z1\[Rule]1248.2,z2\[Rule]1753.61}

findvalues[343.6,229.0,0.371,0.150,1701.8,800,900]

{z1\[Rule]395.884,z2\[Rule]1384.61}